Contract number: C46-49-01

Horizontal and vertical velocity distribution of basalt flows, located in the Enni Formation at Glyvursnes, obtained from refraction seismic analysis

Authors: Uni K. Petersen

Date: 30-12-2010

Relevant technologies for imaging within basalt-covered areas

Budget received so far: DKK 0 (ex. VAT)
Total cost of project: DKK 670,800.00 (ex. VAT)

Date of commencement: 01-04-2010
Date of completion: 31-01-2011

1 Abstract

Basalt velocities are usually obtained from velocity logs and VSP experiments. Here, velocities are established from surface seismic data, on a ~1500 m long combined airgun/dynamite-geophone/streamer profile, by refraction seismic tomography based on ray theory.

In addition to establish the mere velocity distribution, the intent is also to contribute to the general understanding of velocities in successive basalt flows, and to investigate the applicability of the used tomographic method in basalt covered areas. Geological mapping in the area, and velocity logs and VSP data from a 700 m deep well are used for comparison to the tomography.

Best results were obtained with a 50x20 (horizontal x vertical) grid points. This equals 30x20 m grid spacing. The inversion was in two steps: first a coarse starting model was made from inverting with a high regularization parameter (large smoothing) and then an inversion with very low regularization parameter (very little smoothing) was used to arrive at the final result.

The resulting model gives the velocity distribution down to ~200 m depth. In areas where layers are crossing the surface/seabed at a sufficient dip, the modelled velocities are consistent with mapped geology in the area. Whilst below seabed, the dip and location of layers identified from the velocity distribution is ambiguous.

The uneven ray density distribution and thereby following less constraint on the velocities in some areas of the model, is assumed to be of significance for the ambiguity of the velocity distribution below seabed. Also as a result of ray theory, a positive vertical velocity gradient is suspected to be imposed on the solution as an artefact

Comparison to velocity logs and to VSP interval-velocities confirms the modelled velocity distribution as being valid for scales of 100 m. Best conformity was found at ~150 m depth.

An inconsistency between VSP travel times and travel times from velocity log is solved by Backus averaging of velocity logs to 25 m intervals. This is an expression for that the relevant scale for the VSP signal is 25 m.

Based on Backus averaging, the vertical P-wave velocity is expected to be lower than the horizontal P-wave velocity whilst a similar comparison between VSP interval-velocities and modelled velocities leads to the opposite conclusion. This result can however be affected by the inversion algorithm imposing a positive vertical gradient.

The inversion method is pushed to its limits when used on surface seismic data in areas with complex velocity distribution and non-positive vertical velocity gradients. Well defined velocity properties of layers can only be expected to be found in areas where layers are crossing the surface/seabed.

Content

1 ABSTRACT 2

2 CONTENT 3

3 INTRODUCTION 4

3.1 METHODOLOGY 4
3.2 THE DATA 6
3.3 POSITIONING 8
3.3.1 Navigation 8
3.3.2 Positioning the streamer 8
3.4 DETERMINE THE PROFILE LOCATION, (BINNING) 14
3.5 TOPOGRAPHY AND BATHYMETRY 16
3.6 POLARITY STANDARDS 17
3.7 ZERO TIME 18
3.8 BAND-PASS FILTER 20

4 RESULTS 21

4.1 INPUT PARAMETERS 21
4.2 INVERSION 24
4.3 ERROR ESTIMATES 32
4.3.1 Independent uncertainties 33
4.3.2 Dependent uncertainties 35
4.3.3 Root Mean Square 40
4.4 CORRELATION TO GEOLOGICAL INFORMATION 41
4.4.1 Correlation to the surface mapping of the Glyvursnes area and to the lithology in the Glyvursnes-1 composite well log 41
4.4.2 Quantitative correlation to velocity well logs 47

5 INTERPRETATION/DISCUSSION 53

6 CONCLUSIONS 57

7 FUTURE PLANS 57

8 ACKNOWLEDGEMENTS 60

2 Introduction

Since the beginning of the hydrocarbon exploration in the Faroes area the sub-basalt imaging problem has been recognized as one of the major risk-factors.

The problem in obtaining sub-basalt information from reflection seismic data has usually been attributed to the physical properties of basalt, which are very different to those of the overlying and underlying sediments and which have large local variations, usually cause poor transmission of energy, scattering, strong multiple reflections, multiple mode conversion and low-pass filtering of the energy that propagates through a layer of stacked basalt flows (e.g. Ziolkowski *et al.* 2003;White *et al.* 2003).

Later work has shown that although the seismic signal deteriorates as described above when propagating through section of successive basalt flows, there is still sufficient primary energy from below the basalts for sub-basalt imaging. The problem reduces to focusing of the primary energy (e.g. Gallagher and Dromgoole 2008). Whatever processing sequence is used, the focusing of primary energy is based on improving the velocity models used for processing.

Obtaining better velocity models for the processing is an important parameter in improved sub-basalt imaging. Gallagher and Dromgoole (2008) state this clearly when they write: “This [i.e. determining the final velocity field] is one of the most important aspects of sub-basalt seismic processing.”

The aim of this project is to contribute to the understating of the velocities of successive basalt flows. The quantitative information on the velocity distribution of a basalt section in an area where the basalt succession is well described can be used as a constraint when generating velocity models for basalt succession in other areas. Further the aim is to provide a velocity distribution of the area that can be used for the mapping of the uppermost basalt flow units at Glyvursnes.

2.1 Organisation of the report

The report is written following the *SINDRI Reports - Guide for Authors*. All seismic gathers and modelled travel times are included on a DVD as pdf-files.

2.2 Methodology

Strictly speaking, the tomographic inversion of refraction seismic data is a matter of inverting travel times to a velocity model. That means: Which velocity distribution does a model need to have in order to produce travel times that obey the observed travel times?

A condition for finding a solution is that the travel times can be related to a parameterised model. A way to parameterise the model is to divide it into cells – or gridding the model. Other methods of parameterisation could be Fourier transform or τ-p transform but these have constraints on possible source-receiver configurations. The total travel time for a certain source-receiver pair is then a summation over the time spent in each cell.

$$t_i = \sum_{j=1}^{M} \Delta s_j \, p_j$$

Equation 1

Where t_i is the travel time for a certain source-receiver pair and M is the number of cells in the gridded model. Δs_j is the travelled length in cell j of the model and Δp_j is the slowness in cell j of the model.

The inversion of travel time data is the matter of finding p_j. But the travelled distance Δs_j in each cell is unknown.

By imposing modelled travel times from an initial model a travel time residual can be expressed by

$$\Delta t_i = \sum_{j=1}^{M} \Delta s_j \Delta p_j$$

Equation 2

Where Δt_i is the difference between observed and modelled travel time, and Δp_j is the difference in slowness for the initial model and the sought model. In matrix form this is

$$\mathbf{A}\Delta\mathbf{m} = \Delta\mathbf{t}$$

Equation 3

$\mathbf{\Delta t}$ is a vector containing the travel time residuals for all source-receiver pair, $\Delta\mathbf{m}$ is the model residual consisting of all Δp_j and $\mathbf{A}$ is a ($i_{max}\, x\, j_{max}$) matrix of Δs. The matrix $\mathbf{A}$ is determined from the initial model

Subtracting $\Delta\mathbf{m}$ from the initial model $\mathbf{m_0}$ will then give a model more consistent with the observed travel times.

The sought $\Delta\mathbf{m}$ vector is not found from matrix inversion due the high computational cost. Instead an error function is designed

$$\Phi(\Delta\mathbf{m}) = \left\| \mathbf{A}\Delta\mathbf{m} - \Delta\mathbf{t} \right\|^1$$

Equation 4

This is a general formulation of the problem.

The inputs for Equation 4 are the wave paths calculated from an initial model and the travel times from the first breaks arrivals.

It is widely used to calculate the wave propagation based on ray theory. This offers an efficient (computer cost) method for doing the job. However, ray theory is a high-frequency approximation and does not account for diffraction effects.

Ray theory is in fact only accurate for modelling anomalies down to the scales of the first Fresnel zone, i.e. a few wavelengths (Williamson 1991;Williamson and Worthington 1993). Alternative methods obtaining wave paths and travel times have been suggest by various authors (e.g. Vasco *et al.* 1995;Cerveny and Soares 1992).

The WARRPI program package used for the current project is based on the inversion scheme outlined in Equation 4. The following is an outline of the inversion algorithm. For details on the inversion algorithm I refer to Ditmar et al. (1999).

The error function in Equation 4 is sensitive to noisy data, as the model parameters will be unrealistic high or low in order to satisfy the erroneous travel times. Therefore some kind of smoothing is used to lessen these effects (Phillips and Fehler 1991).

In the WARRRI algorithm the smoothing is applied with a regularisation condition *R*. The intensity of the regularization is controlled by a Velocity Regularisation Parameter α (Equation 5).

$$\Phi(\Delta\mathbf{m}) = \left\|\mathbf{A}\Delta\mathbf{m} - \Delta\mathbf{t}\right\|^1 + \alpha R$$

Equation 5

The regularisation condition is as follows:

$$R = \int_{\Omega_1}\left[10\left(\frac{\partial n(x,z)}{\partial x}\right)^2 + \left(\frac{\partial n(x,z)}{\partial z}\right)^2\right]dxdz$$

Equation 6

Ω_1 is the area covered by the velocity grid and *n* is the model vector $\Delta\mathbf{m}$**.** The regularisation condition is thus an expression for the magnitude of the change of the model vertically and horizontally. The factor 10 in the first term accounts for that vertical variations are more probable than horizontal ones.

The wave paths and travel times necessary for the inversion are calculated from ray theory with the SEIS83 code (Cerveny V. and Psencik I. 1984). The current project represents a shallow, small scale profile, where the heterogeneity of the profile in investigation is expected to have large variations within small distances. Therefore the issue of the limitations ray theory for refraction tomography is definitely an issue here.

The deteriorating effect of the shortcomings of ray theory is expected to have its largest effect in areas with low ray coverage, while areas with large angular coverage are expected to be less influenced.

Finally, it should be emphasized that the solution to the inversion is non unique. This implies that the solution must be viewed in relation to expected geology and other a priori information in order to disqualify unrealistic models.

2.3 The data

This refraction seismic analysis is based on a reflection seismic profile from the SeiFaBa 2003 acquisition (Petersen *et al.* 2006;Andersen *et al.* 2004).

The initial profiles, GBX602 and GBXDYN, form a combined profile that has some qualities that make it well suited for performing shallow refraction seismic analysis. It

has a relatively long offset, two-way shooting and it is centred at the Glyvursnes-1 well (Figure 1).

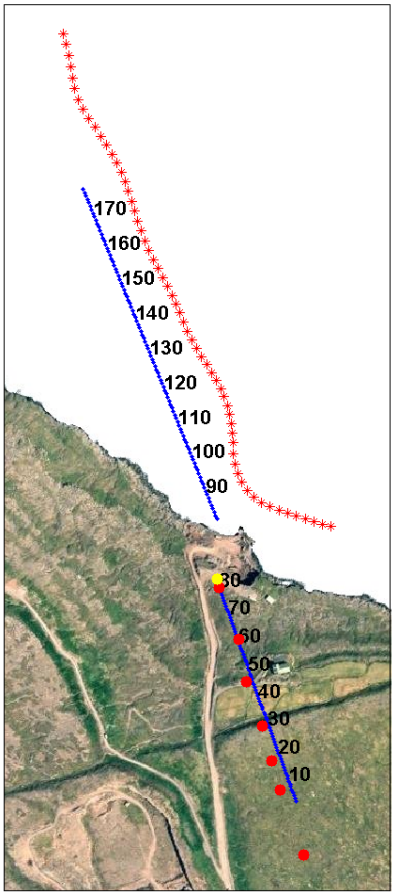

Figure 1 Acquisition layout of the GBX602 and GBXDYN profiles. Red points onshore are dynamite shot positions and red points offshore are airgun shot points. Blue points onshore and offshore are geophone and hydrophone positions. Yellow dot marks the positions of the Glyvursnes-1 well.

The total offset of the receiver layout of the profile is 1086 m, comprised of a 400 m geophone layout and of a 600 m streamer layout. Station interval of geophones is 5 m with every fourth geophone being a 3C geophone. Group interval of streamer is 6.25 m.

The sources are a 160 in^3 airgun cluster with shotpoint intervals between 15-20 m and 250 g dynamite charges in 3 m deep holes with shotpoint intervals between 50-100 m. The maximum source-receiver offset is 1343 m

Both dynamite shots and airgun shots are recorded on both geophones and streamer simultaneously. The recorded length is 3 s sampled at 0.5 ms.

During the modelling a third profile was included in order to balance the ray-coverage. The profile in question is the Seifaba-01 profile with a geophone layout that coincides with the dynamite shot points on Figure 1. The geophone layout is 600 m with 5 m station intervals. The shot points along this profile are with 10 m intervals.

The 700 m deep Glyvursnes-1 well gives velocity information in the form of the zero offset VSP and velocity logs. The VSP source is a 150 in^3 airgun fired in a specially

constructed pond with water depth of about 1.5 m. The offset from the pond to the well was 14 m. The VSP receiver is a 3-component down-hole geophone, clamped with a hydraulic system, recording at 10 m intervals from 50 m to 600 m depth (Shaw 2006).

The log data from the Glyvursnes-1 well concerns the GEUS processed full waveform velocity logs (Waagstein and Andersen 2003) and the bulk density log re-calibrated to measurements on core samples (Waagstein, unpublished data).

	Start depth	Stop depth	Sampling interval	File
	m	m	m	
Density	2.93	698.83	0.1	Gl1-dens.txt
Vp	5.6	597.4	0.2	GL1-FWS_GEUS.LAS
Vs	5.6	597.4	0.2	GL1-FWS_GEUS.LAS

Table 1. Well logs used in the project

2.4 Positioning

2.4.1 Navigation

The land navigation of the GBX survey is with accuracy in the order of ±0.05 m whilst the accuracy of the Seifaba-01 is lesser - in the order of ± 1 m[1]. The tugboat and gunboat navigation is with an accuracy of ±2 m. For more details I refer to the acquisition report (Andersen, Worthington, Mohammed, White, Shaw, and Petersen 2004).

2.4.2 Positioning the streamer

The streamer location can be determined from the location of the two endpoint positions established by the tugboat positions and the jack-up rig position and this has been done so in previous reflection seismic processing (Petersen, Andersen, and White 2006;Japsen *et al.* 2006).

The distance from the tow point on the tug boat to the closest channel on streamer is 44 m and the distance from the edge of the jack-up rig to the closest channel on the streamer is 4 m (field notes saved in *streamer_set_tugboat.doc* file). With known dimensions of gangway and jack-up rig this allows for an apparently accurate positioning of the streamer (Figure 2).

There are however two main factors that can significantly deteriorate the accuracy of the streamer position. Firstly the tidal current imposes transverse forces on the streamer, resulting in the streamer forming curved positions rather than forming a straight line. The second factor relates to the navigation system on the tug boat. The system determines the tow point of the streamer by a preset offset relative to the GPS antenna and from the sailing direction of the boat. But since the tugboat doesn't have any preferred sailing direction, the measured tow point is scattered around the GPS antenna positions.

[1] Originally measured with a Garmin 76 and later (2009) improved with a Leica TC 1600 Total Station for high accuracy surveying.

Figure 2. Setup of the GBX streamer. The shore position of the gangway was measured. The length of the gangway is 15 m. The dimensions of the jack-up rig are 7.6 x 12 meters. The arrow marked A is the tugboat keeping the streamer in position and the arrow marked B is the gunboat. During the GBX602 survey the gunboat was passing the streamer at distance of about 50 meters. Pay attention to that the streamer is not in a complete straight position due to tidal currents. The picture is taken from the position of Glyvursnes-1 well facing Tórshavn.

In this modelling, the positioning of streamer will be sought improved by placing it relative to travel times from the direct arrivals from shot points.

Picks of first direct arrivals establishes the distance from each shot point to nearest streamer location. Doing this for all shot-points will outline the location of the streamer. The two main parameters to establish are the zero time of the gathers (or which phase to pick on the signature) and the speed of sound in seawater.

For salinity and temperatures relevant for the present acquisition the velocity of sound in water is about 1480 m/s.

The zero time of the gathers is established by analyses on common receiver gathers (Figure 3). Each travel time represents the distance from a shot point to the receiver location. So when plotting the shot-point receiver distances as circles around the respective shot points, ideally they will converge at the receiver position. If they don't this is an indication of wrong zero-time and the picks can be time shifted as to produce the best convergence.

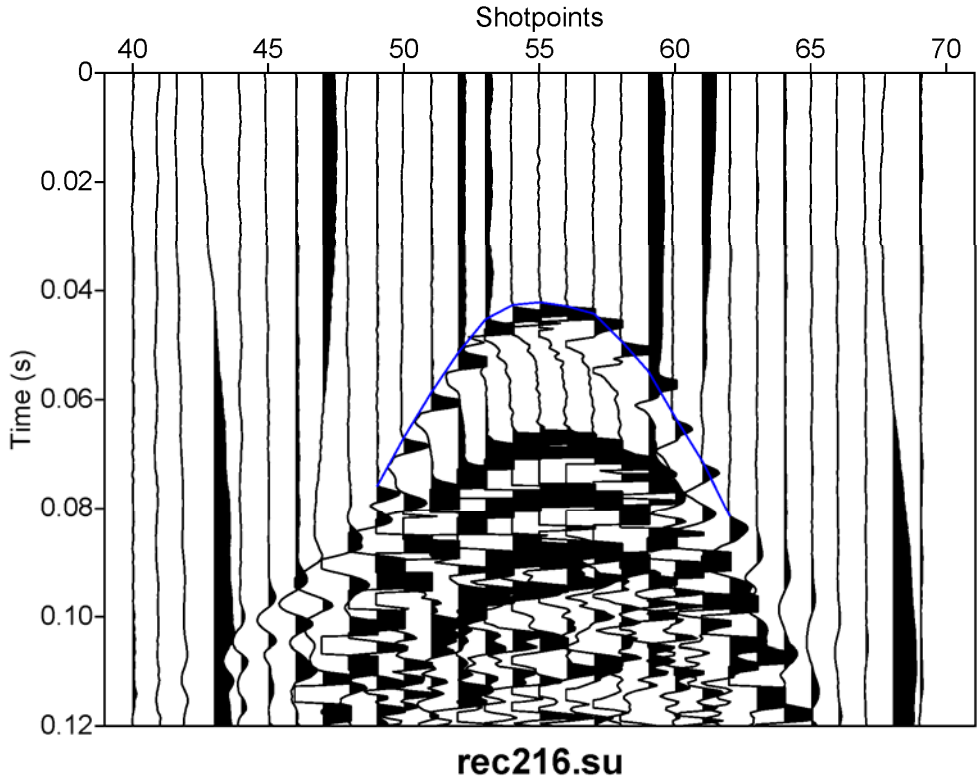

Figure 3. Receiver gather 216. Blue annotation shows picks of first direct arrival.

Figure 4 shows the effect of time shifting in steps of 4 ms for four selected groups along the streamer. Except for receiver number 160 they all show best convergence with a time shifting of 6 ms. Receiver 160 has better convergence with less time shifting than 6 ms. For channels lower than receiver number 160 the streamer is at so shallow water that the refracted waves arrive before the first direct arrival so that it can not be picked with confidence. The reason for why receiver 160 does not favour same time shifting as the other gathers is not fully understood.

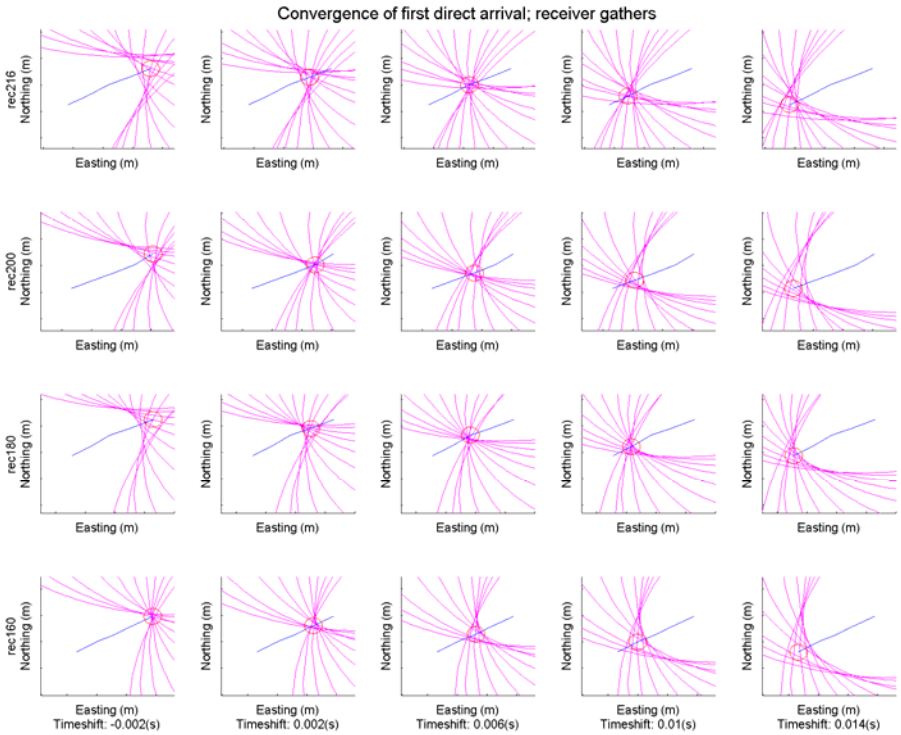

Figure 4. The figure shows travel times converted to distance and plotted as radius around respective shot points (magenta colour) for four different receivers gathers. The effect of time shifting the picks is shown for five different time shifts. The spatial size of all plots is the same and for each receiver the location is the same so locations can be compared between figures for respective receivers. The red circles annotate estimated best fit of receiver location. The radius of red circles is 3 m. Blue lines show how receiver locations vary with different time shifting. The receiver locations vary perpendicular to the streamer.

Based on the picks of first direct arrivals on shot gathers, water velocity of 1480 m/s, time shifting of 6 ms. and the jack-up rig position, the location of the streamer was established. The channel positions along the streamer were established by determining the location of one channel (channel 216) based on a receiver gather analysis (Figure 4) and then place channels with 6.25 m group interval along the streamer location (Figure 5).

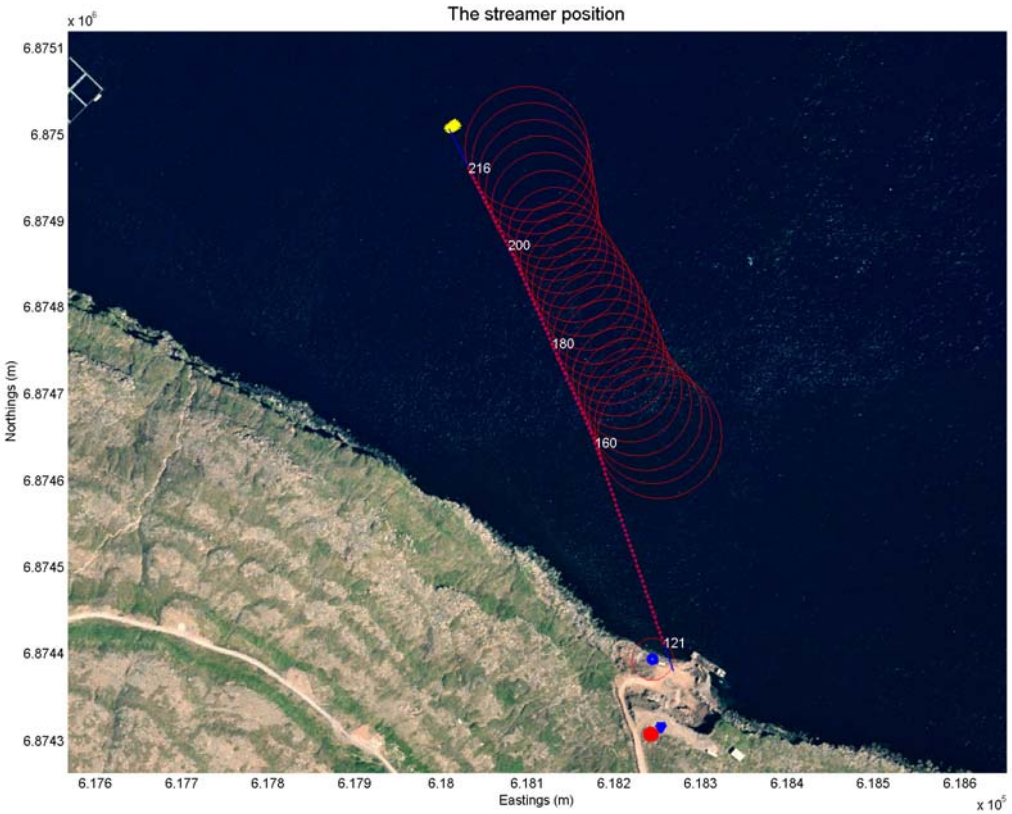

Figure 5. The estimation of streamer position from neareast offset picks. Position of Glyvursnes-1 (blue triangle) and the zero-offset VSP pond (red solid cirkle) are plotted for reference. Yellow area represents tugboat position during acquisition of GBX602. The red circle close to channel 121 marks the distance from the measured gangway position (blue dot) to the edge of the jack-up rig.

QC of the channel positions was done by comparing these positions to the positions established by locations relative to tugboat and jack-up rig.

The distance between tugboat and the closest channel on the streamer is estimated to be around 49 m. This is somewhat larger than the 44 m noted in the field notes (Figure 6).

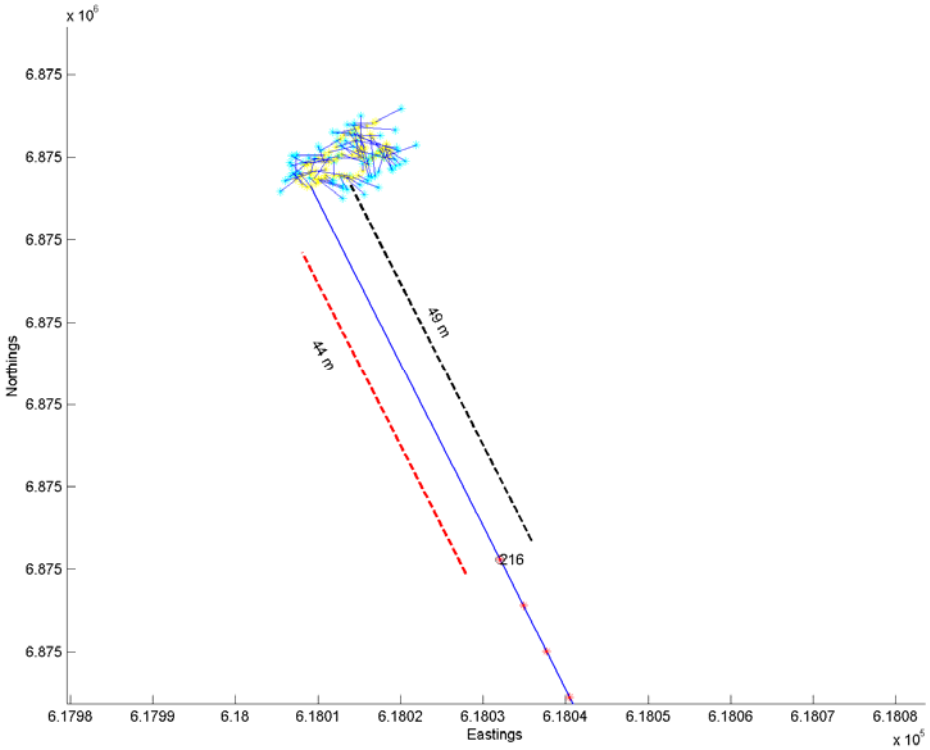

Figure 6. The northern endpoint of the streamer. Yellow points are the tugboat GPS antenna position during the GBX602 profile, cyan points are the positions of the tow point of the streamer. Blue lines connect the respective measurements. Red points are channel positions. Black and red stipulated lines show distances.

Further, on the end towards the jack-up rig, the closest channel ends up being inside the jack-up rig and not at a distance of 4 m as stated in the field notes. But this depends very much on where the intersection with the edge of the jack-up rig is defined (Figure 7).

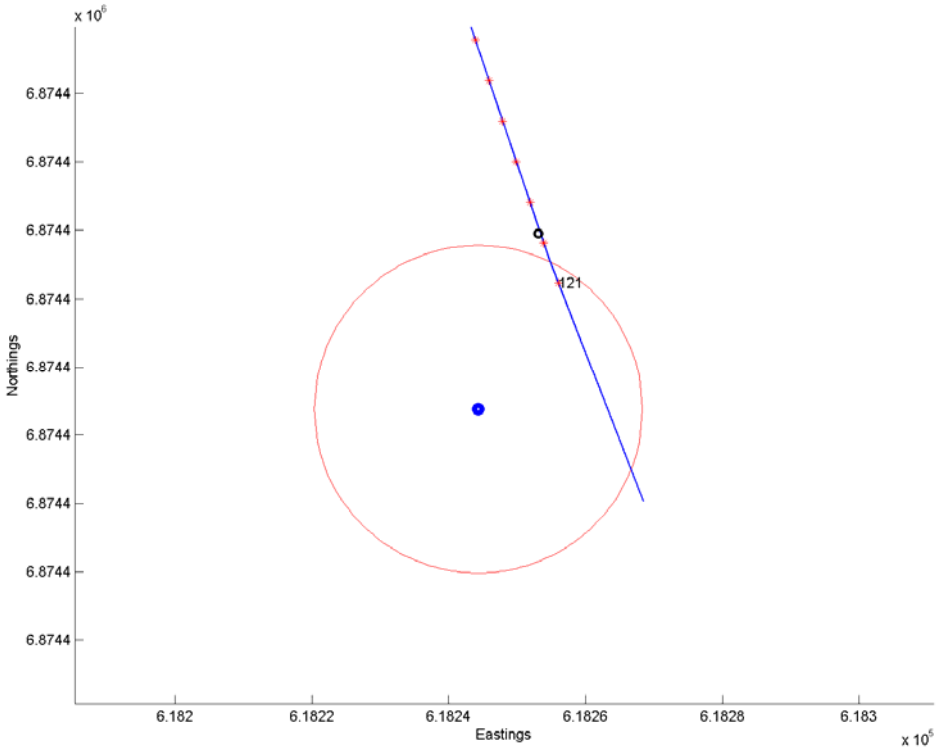

Figure 7. The southern endpoint of the streamer. Red points mark channel positions. Blue point is location of gangway onshore. Red circle is the distance from shore location of gangway to the edge of the jack-up rig derived from the dimensions of the gangway and jack-up rig. Intersection between streamer and edge of jack-up rig is from inspection of Figure 2 and Figure 5. Black circle marks 4 meter distance from edge of jack-up rig along the streamer.

All in all the streamer location is apparently shifted about 5 meters to the south relative to the tugboat and jack-up rig positions. Reasons for this difference has been sought but not found so the continued analysis will be with the streamer positions established as described above relative to shot point positions.

2.5 Determine the profile location, (binning)

The input for the modelling program is a 2D profile of the area. Whilst the shot point positions are projected directly onto the 2D profile, the receiver positions are determined from the shot-receiver offset relative to the projected shot position.

In the ideal case, were shot points and receiver points all lay in the same profile/cut, this poses no problems. But when, as in the present case, some shot points are with a significant offset towards the receiver layout (Figure 8), there will be an inconsistency between the position of the receiver in the 2D model and the source-receiver offset. Either, one has to choose correct offset and wrong receiver position or one has to choose wrong receive position and correct offset.

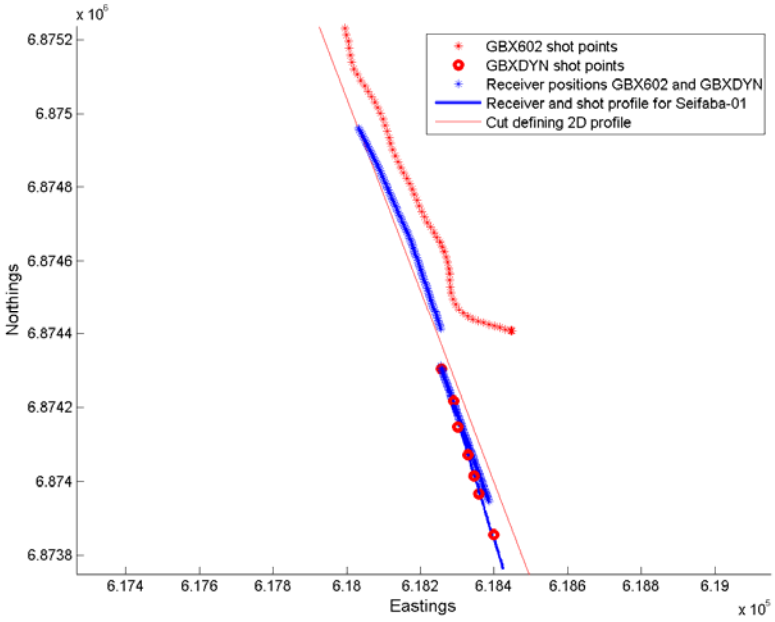

Figure 8 Positions used for generating the 2D topography, bathymetry, shot and receiver positions.

Since a wrong offset leads to wrong velocities the approach is to keep the correct offset on behalf of wrong receiver positions.

The effect of wrongly projected receiver positions is illustrated by Figure 9. The figure shows the projected receiver positions for all GBX602 and GBXDYN shot gathers. Although we know, that in reality the receiver positions are at the same location for all shot gathers, the receiver positions projected onto the 2D profile, while demanding correct offset to shot positions, do vary significantly between shots. The seismic traces related to these shot-receiver combinations contain the correct velocities but in the wrong location so to speak.

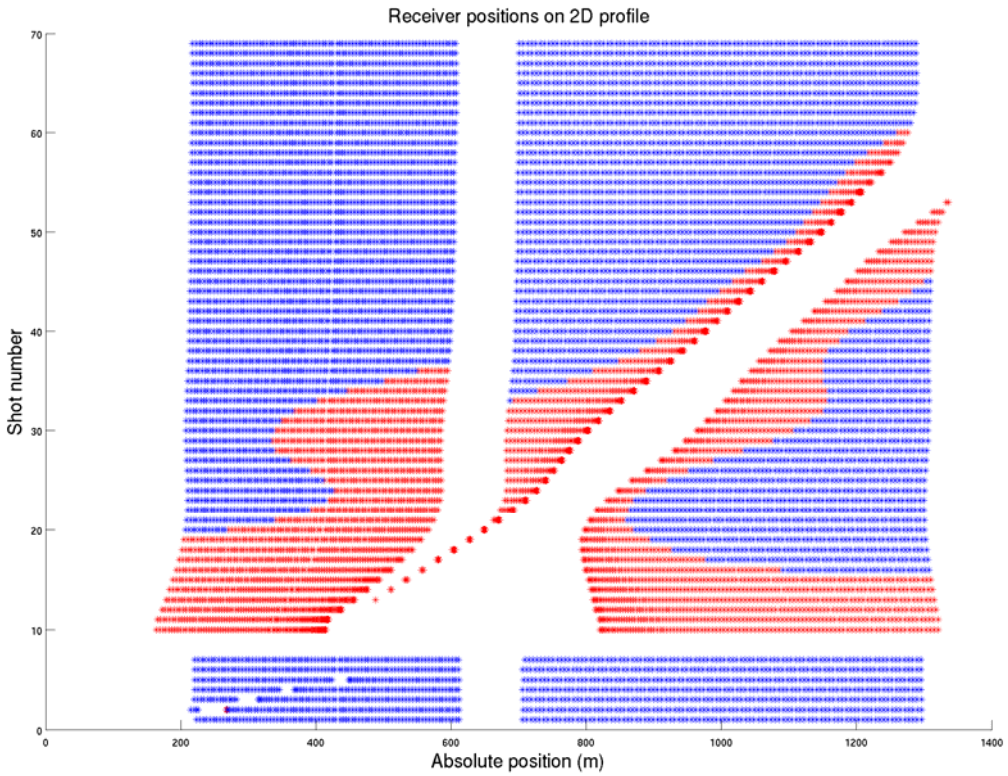

Figure 9. Receiver positions for all shot gathers projected onto 2D. Red positions mark receivers with larger deviation than +/- 15 m relative to the receiver positions projected directly onto the profile.

The receiver positions on the 2D profile were compared to the correct receiver positions (receiver positions projected directly onto the profile cut). In the present modelling I accept deviations of up to ±15 m from the correct positions. Traces belonging to receivers with larger deviation are rejected. It is considered to be a relatively large deviation but it is a trade off since a smaller deviation would lead to abandoning too much data.

2.6 Topography and bathymetry

The initial model is designed from the topographic and bathymetric information of the modelled profile (see Figure 8 for location of profile).

The topography of the land profile is accurately defined due to the high accuracy of the land navigation and due to that the shot points coincide with the geophone layout.

The depth at all airgun shot points was recorded from sonar during acquisition and is part of the navigation log files (Figure 10). So the bathymetry can be extracted for any position.

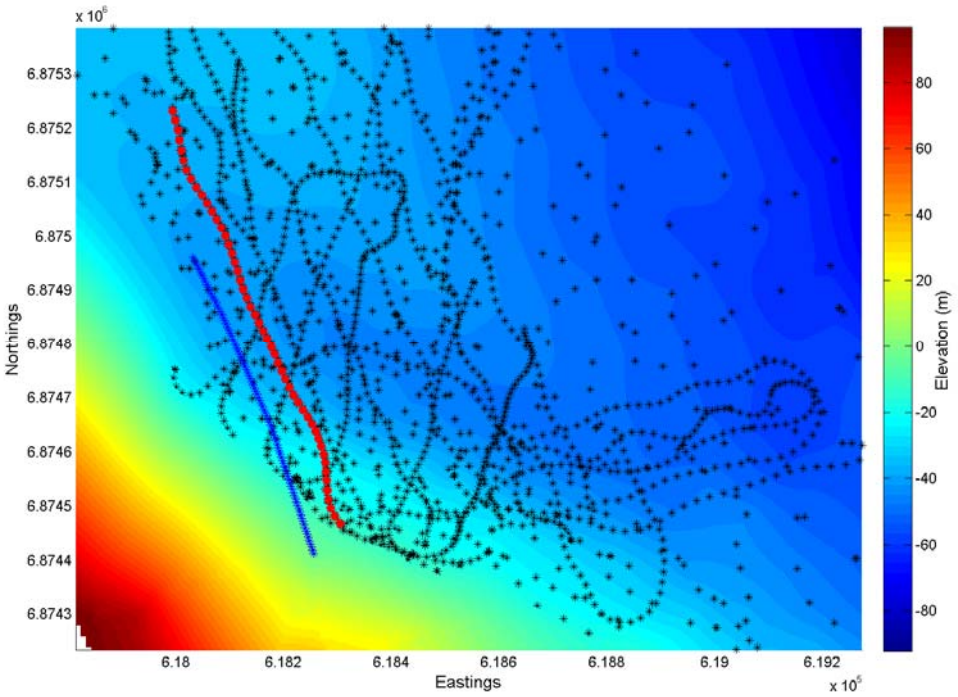

Figure 10 Black points show shot points used for generating the bathymetry for the area. Blue points show location of the streamer and red points show the GBX602 shot points.

The fact that the sail line for the shot points has an offset to the streamer layout has a significant effect on the ambiguity of the bathymetry. For parts of the profile there are depth differences of up to 10 m (Figure 11).

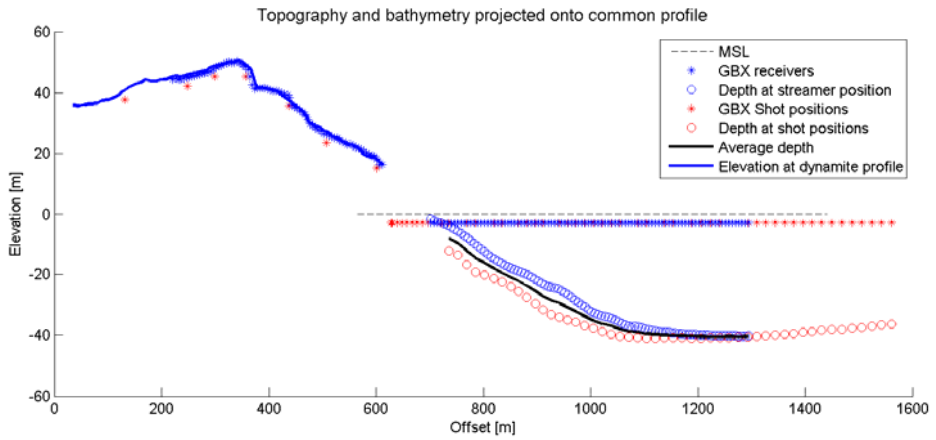

Figure 11 Elevation information used for generating the model. The depths are extracted from the bathymetry information shown in Figure 10.

This poses a problem for the designation of the bathymetry. There is no correct solution whether the depths for the shot points or for the streamer should be used. In the absence of a better solution the average depth will be used.

2.7 Polarity standards

The SEG normal polarity standard for seismic data specifies that the first break from an explosive source is represented by a negative number (Thigpen *et al.* 1975;Brook *et al.* 1993).

In the case of a positive reflection coefficient or of the direct arrival this implies negative amplitude for a minimum phase wavelet and positive amplitude for the central peak of a zero phase wavelet. The raw data used for this project are considered to be minimum phase.

Negative values are plotted as troughs (wiggles going to the left and not filled) and positive values as peaks (filled wiggles going to the right). Inspection of data shows that while the geophone recordings show troughs for the first break arrivals according to the SEG normal polarity standard the streamer recordings show peaks for the first break arrivals. On the preparation of data the polarity of the streamer recorded data was thus reversed so the data now comply with the SEG normal polarity standard.

2.8 Zero time

The dynamite and airgun data are acquired on triggered signals from the triggering of the source. So as such the data have proper zero time. Zero time was however re-established directly from data due to this being a case of a small scale profile very sensitive to small systematic errors.

The zero-time of the airgun data was established by analysing of direct arrivals on receiver gathers, see chapter 2.4.2. There it was shown that most consistency of the picked direct arrivals was obtained by time shifting the data 6 ms.

In order to follow the SEG normal polarity standard, and in order to have same recording convention as on the dynamite data, the streamer data where polarity reversed. It was desirable to identify events at the first trough-peak zero crossing. With polarity reversed data, a time shift of – 4 ms leads to that event shall be picked at the first trough-peak zero crossing (Figure 12).

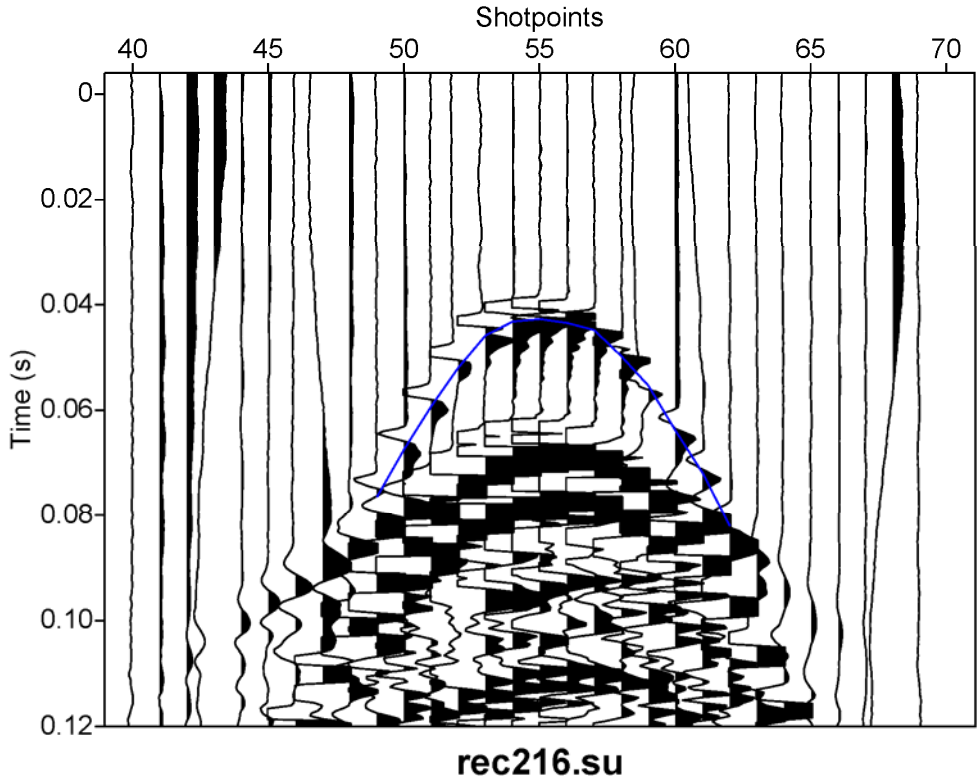

Figure 12 shows the same picked travel times as in Figure 3 but now time shifted 6 ms downwards. The traces are now plotted according to general convention starting with a trough for the first break. The Seismic traces are time shift 4 ms upwards so that the picked time corresponds to the first trough-peak zero crossing.

The zero time analysis on the Sefaba-01 data has been done previously (Petersen 2009). The analysis on the Seifaba-01 data was initially done with SEG reverse polarity and picks were on the first onset. The polarity of the Seifaba-01 was thus reversed and the data were time shifted so the picks compared to the first trough-peak zero crossing as for the airgun data. The GBXDYN data were then compared to the Seifaba-01 data and shifted accordingly. This demonstrates the consistency of the Seifaba-01 data to the GBXDYN data (Figure 13 and Figure 14).

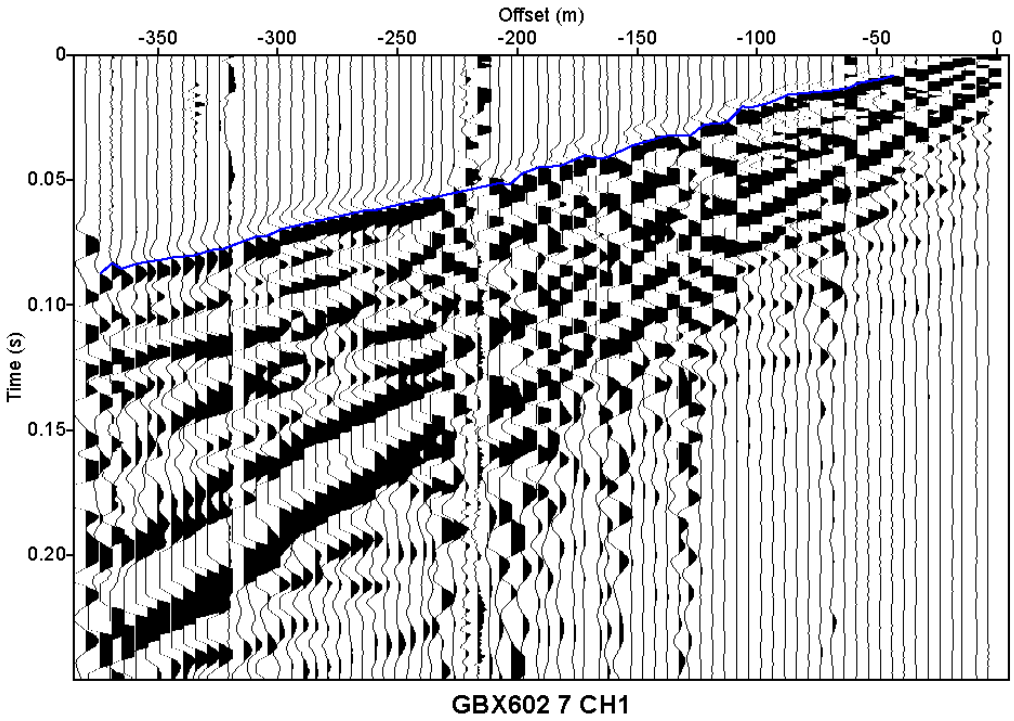

Figure 13. Picks of first break GBXDYN shot gather.

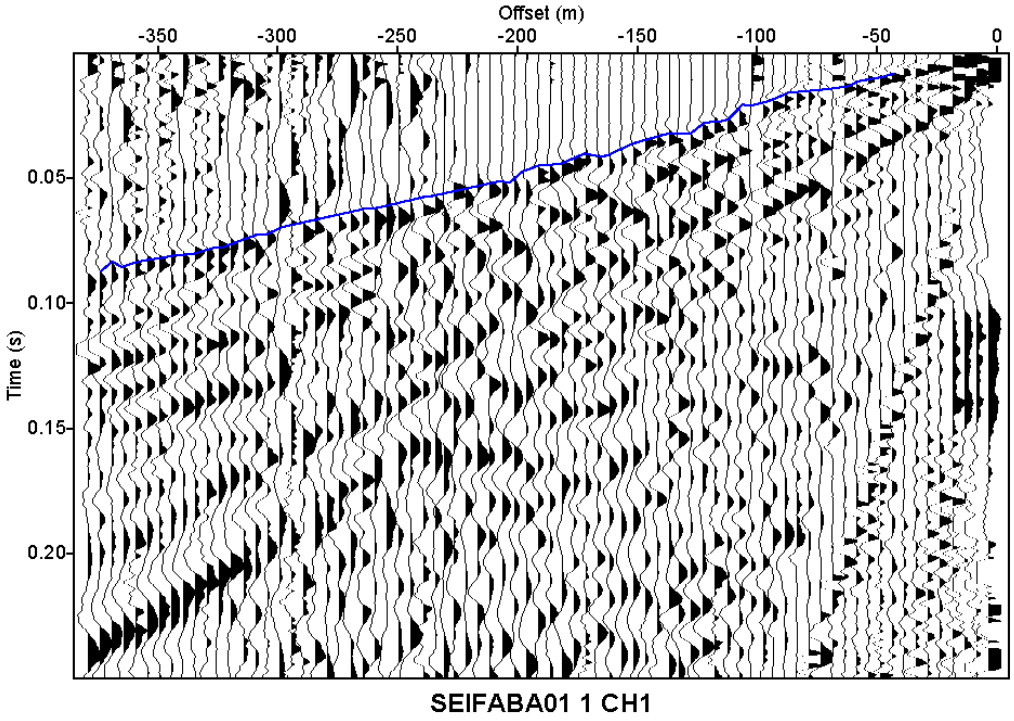

Figure 14 Picks of first break from GBXDYN shot gather (Figure 13) plotted on respective Seifaba shot gather. For this figure, offset is only plotted up to 400 m to compare with the GBXDYN data, while the Seifaba-01 data consist of 600 m offset.

2.9 Band-pass filter

Finally, the effect of band-pass filtering of data had on the location of the through-peak zero crossing was analysed. Figure 15 and Figure 16 show that the location is preserved after band-pass filtering.

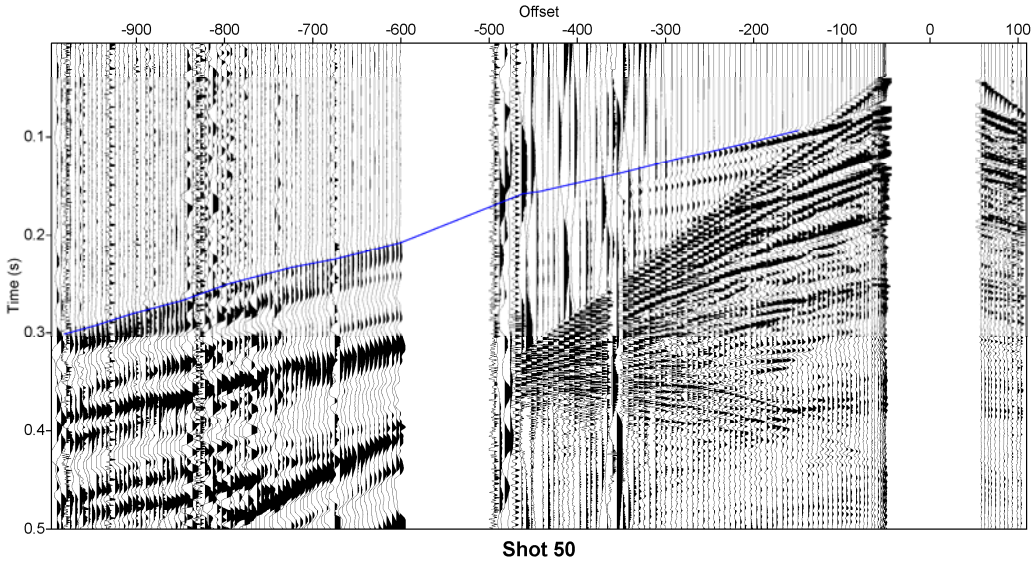

Figure 15. Blue line is through-peak picking from first arrival.

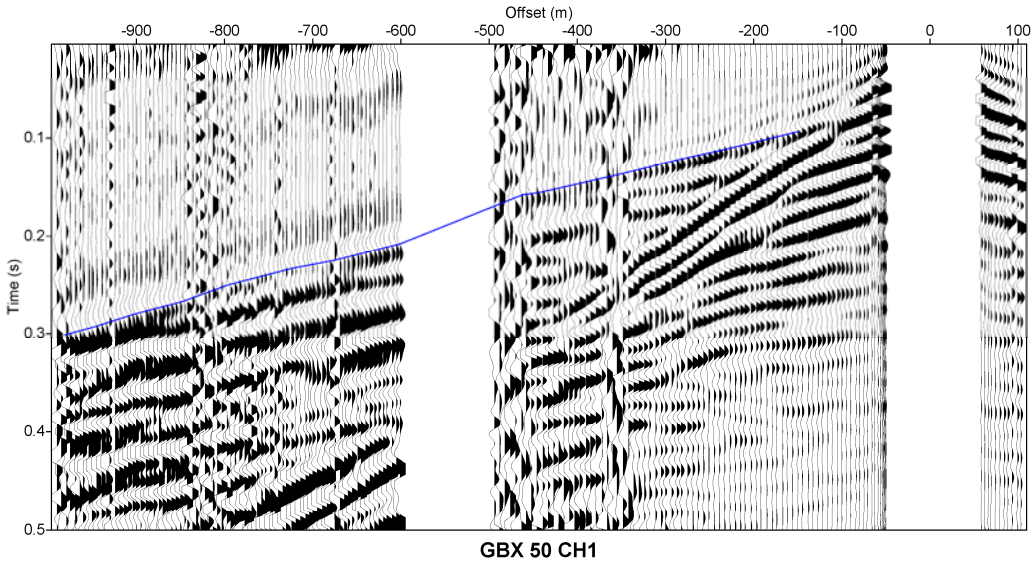

Figure 16 Band-pass filtered 12,14,50,60 Hz. Blue line shows the same picks as for Figure 15.

3 Results

3.1 Input parameters

The first input parameter for the modelling is the initial model defining the geometry for model. This concerns topographic and bathymetric information, and all shot positions and receiver positions. Thus applying all known information to the model.

The current modelling is done as a two-layer model with the layer above seabed as the uppermost layer and the layer below seabed as the lowermost layer. Only first-break events will be considered in the modelling.

To ensure travel times from below seabed, the velocity distribution for the lower layer has a positive vertical velocity gradient. Besides this the velocity distribution below the surface is chosen with no assumptions of prior knowledge.

The second input parameter is defining the shot and receiver locations on the 2D profile and then picking travel times on gathers. The initial model is shown on Figure 17 with the shot point locations for the GBXDYN and GBX602 shootings. The dynamite shot positions are at 3 m depth relative to the surface while the geophones are located on the surface. The airgun depth is at 3 meter depth below the water surface and the streamer depth is also at 3 meter depths. To accommodate this, water surface of the model is set 3 meter below actual depth and the shot depths are set just below the surface of the model.

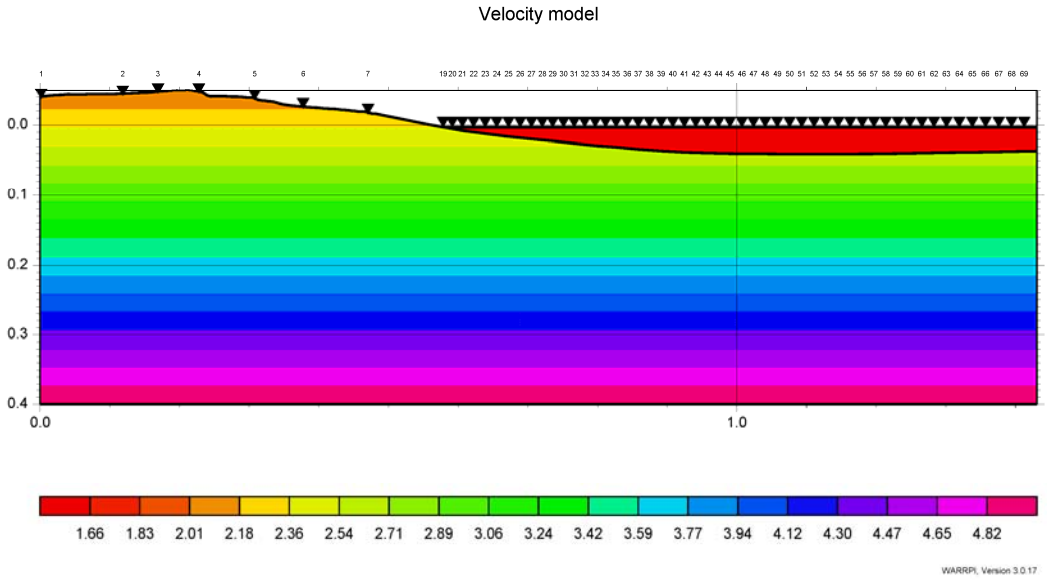

Figure 17 The initial model based on preparation of navigation bathymetric and topographic information for the profile (Figure 11). The water velocity is set to 1.48 km/s.

The WARRPI program package facilitates programs for picking of events in combination with analysing of the modelled travel times. Figure 18 and Figure 19 show examples for picks of first breaks for an airgun shot gather and a dynamite shot gather.

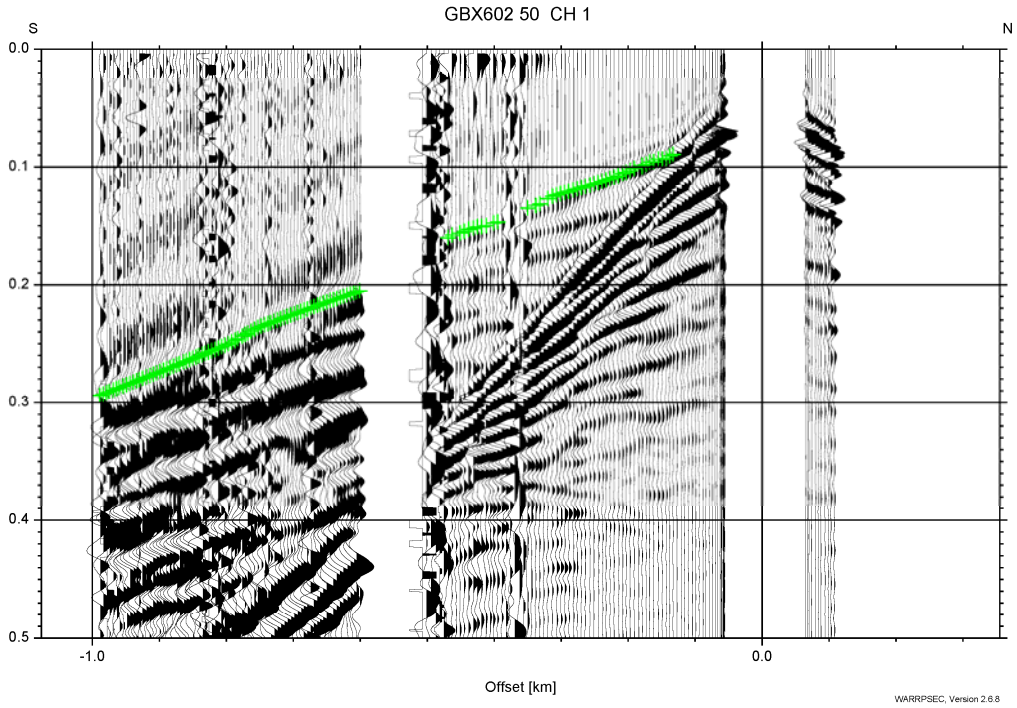

Figure 18. Picks of first breaks on airgun gather (green '+'). The data is band pass filtered at 14-60 Hz. (Seismic Unix butterworth filter: stoplo:12 passlo:14 passhi:60 stophi:90).

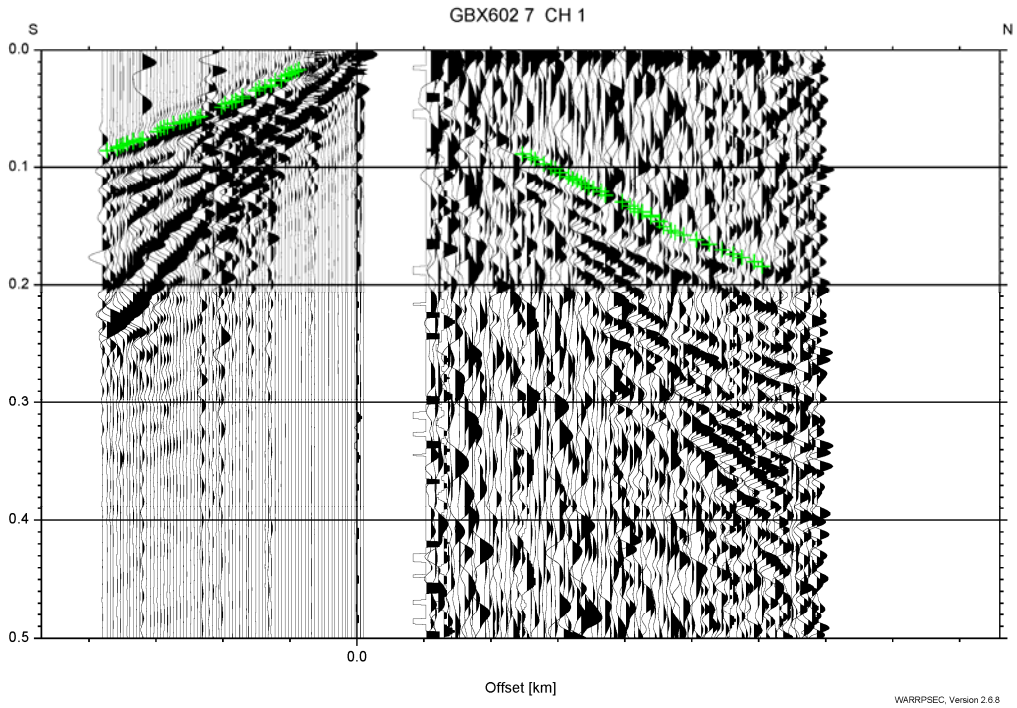

Figure 19. Picks of first breaks on dynamite gather (green '+'). The data is band pass filtered at 14-60 Hz. (Seismic Unix butterworth filter: stoplo:12 passlo:14 passhi:60 stophi:90).

3.2 Inversion

The final results of the modelling reflect the results from about 50 different approaches for inversion. The main consideration during inversion was to arrive at a single model that produces consistent travel times for all gathers.

The parameters to adjust during inversion are:

- Velocity Regularisation Parameter (VRP)
- Objective Function Minimization Parameter (OFMP)
- The gridding of the model

The VRP is a parameter for the fractional change in slowness for each iteration. Defined as α in Equation 5. The OFMP determines at what value the objective function (Equation 5) is sufficiently low.

The gridding of the model shall be considered in relation to the desired resolution of the model. The gridding has to be fine enough to contain the velocity information needed for modelling the seismic wave propagation. A too fine gridding can however result in unstable solutions.

The progression can be summarised as follows:

After initial testing the gridding was set to 50x20 (horizontal x vertical) grid points. This equals to approximately 20 m vertical spacing and 30 m horizontal spacing. The inversion was done, following the paper by Ditmar *et al.*(1999), by starting with a high VRP (e.g. 50) and decreasing it 3-5 times for each iteration and keeping the OFMP at least 100 times lower than the VRP.

Several attempts were made with different VRP and OFMP values. Continuing iterations did never end with a stable solution where the RMS converged to a minimum. At some point the continued modelling with lower VRP always lead to diverging, not realistic solutions. Figure 20 shows a typical solution before the results started to diverge. It shall be noted that the names of the models like e.g. *modeleuqal03* do not have any other meaning in the present context than to uniquely identify the different solutions.

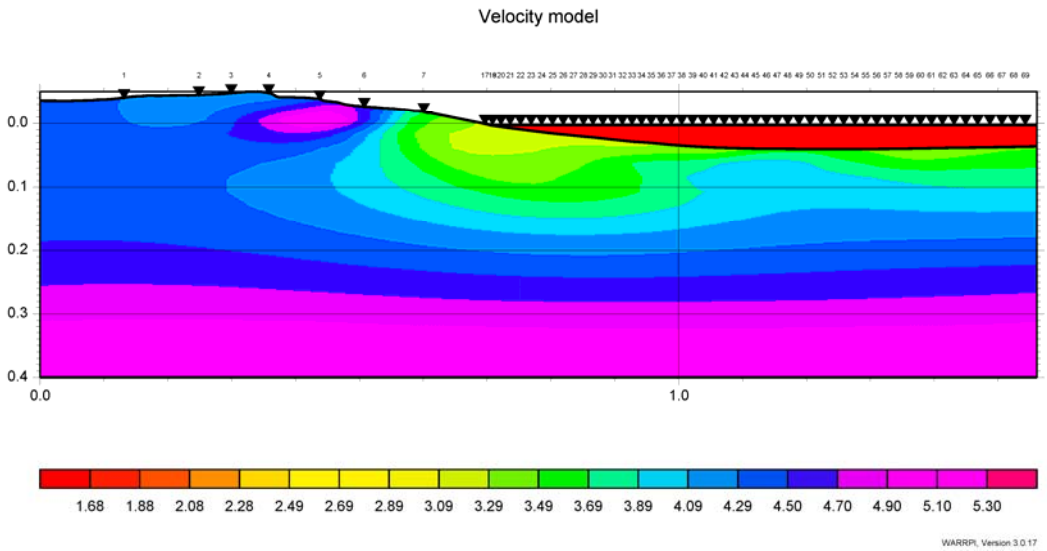

Figure 20. The *modelequal03* solution. Triangles show location of shot points. Velocities on colour bar are in km/s. Axes show distance in km.

The ray density distribution in Figure 21 shows that there is actually little information from the deeper parts. The properties at larger depths of the inverted model where there is no ray coverage, are a result of the initial model in combination with how the Regularization Condition (Equation 5) affects the neighbouring grid points.

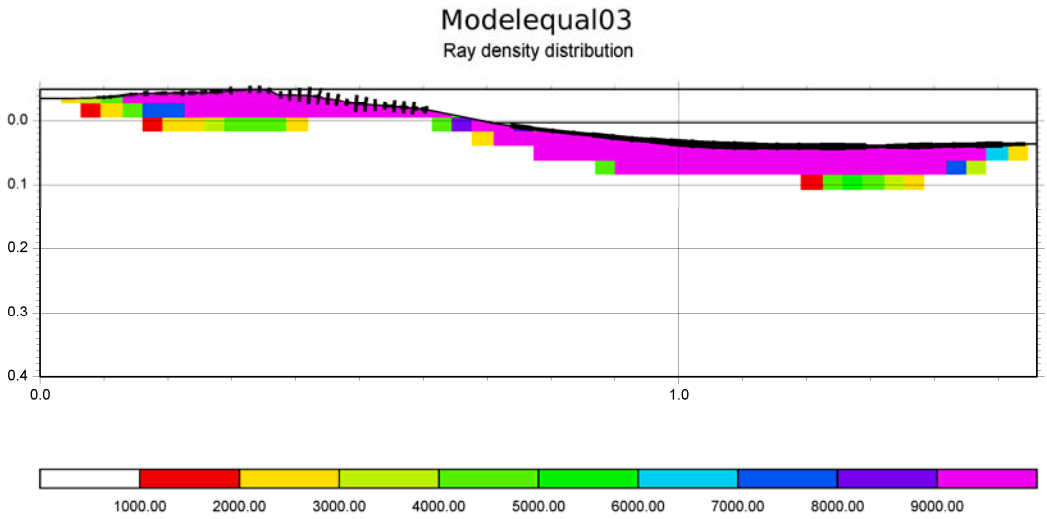

Figure 21. Ray density distributions: The number of rays that cross the cells divided by the horizontal length of the cell. Axes show distance in km.

This solution produced travel times for many of the gathers but there were also several gathers with no travel times at all. Figure 22 shows an example of travel times for a gather.

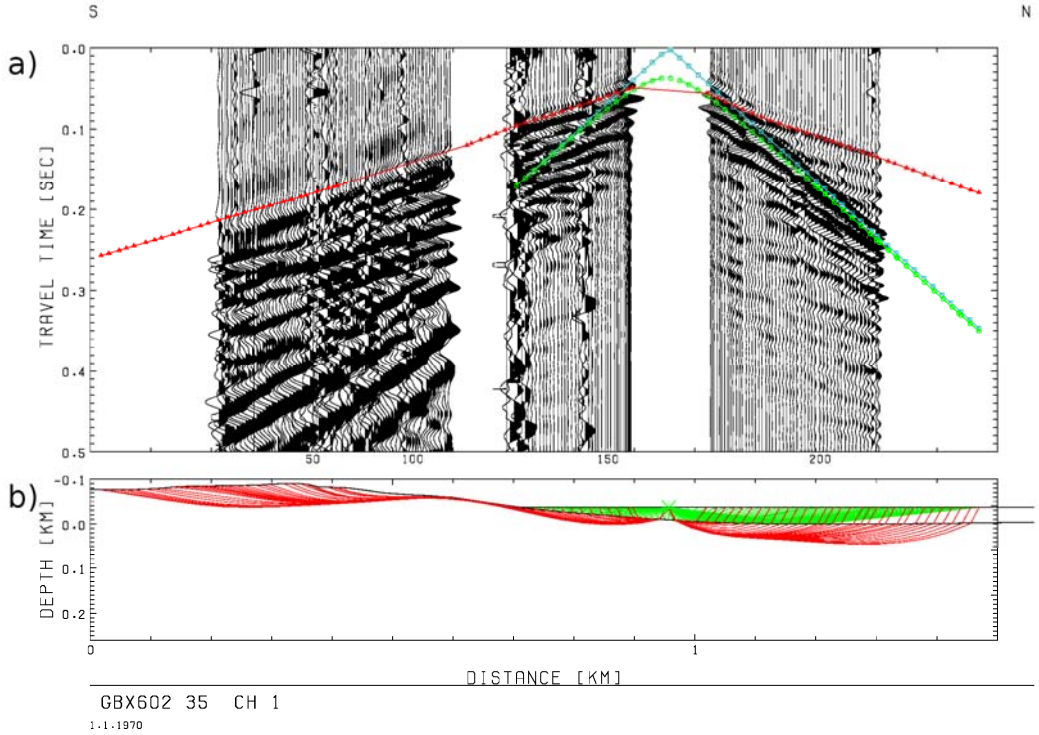

Figure 22. a) Travel times plotted on top of seismic shot gather. b) ray paths for airgun shot point 35. Calculated with *modelequal03*.

The *modelequal03* (Figure 20) does not reflect the expected property distribution of successive basalt flow-units. Ray paths indicate that there is a low-velocity layer as annotated on Figure 23.

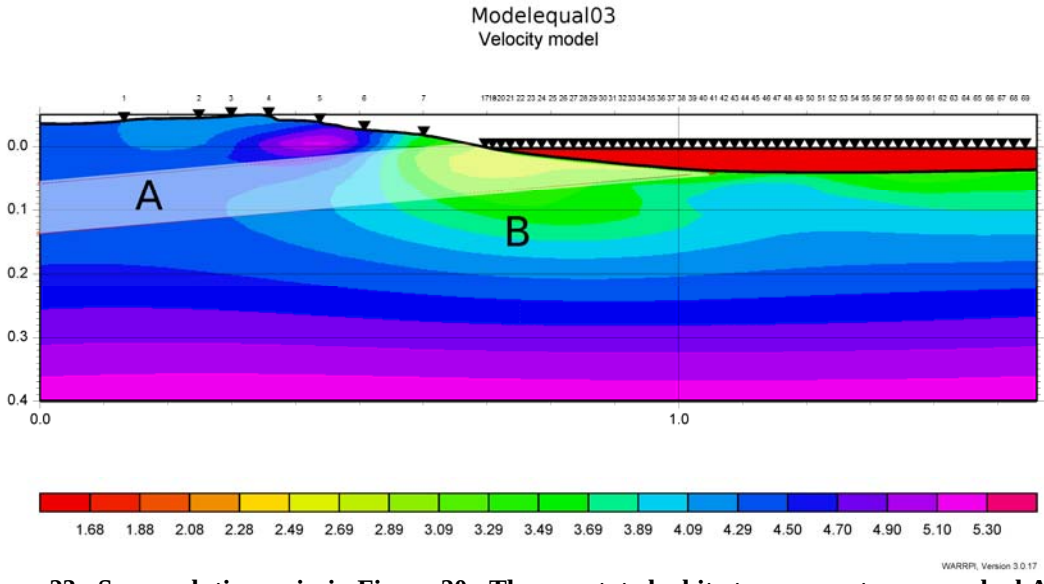

Figure 23. Same solution as in in Figure 20 . The annotated white transparent area marked A is the approximate location of the expected low-velocity zone indicated by data. B marks an area affected by erroneous modelling of the low-velocity zone. Values on colour bar are in km/s. Axes show distance in km.

But although the low-velocity zone is identified it is difficult to model its extent. The handling of a low-velocity zone puts greater demands on the modeling parameters.

The failing to model the low-velocity zone affects the velocities below the low-velocity zone. The errors are inherited, so to speak. In order to produce an overall travel time corresponding to the picked events, a too high velocity in the area marked A in Figure 23 results in too low velocities in area marked B.

The aim of this project is to do an inversion only based on seismic data. This means that information from the velocity logs shall not be included in the initial starting model and that the resulting model shall be an output directly from the inversion algorithm. Therefore no attempts were made to manually adjust the model.

The effect of imbalance in ray paths was considered, having about 50 airgun shots relative to 7 dynamite shots. It seemed like the inversions generally had better convergence of airgun-geophone travel times than of dynamite-streamer travel times.

Inversion was performed with decimated airgun shot numbers in order to balance the ray paths. Although there now was an equally good convergence of travel times from dynamite-streamer recordings as of airgun-geophone recordings, it was considered that the deteriorating effect of using less information was too large.

Instead the seismic data from the Seifaba-01 profile was included in the modelling. This resulted in equally dense coverage of the dynamite-geophone recordings as of the airgun-streamer data. Although the airgun-geophone coverage still was ~10 times larger than the dynamite-streamer coverage.

Now several modelling sequences followed where all means where used to control the convergence of the modelled travel times towards the picked first-breaks. This was done by, for each step, considering effects of the following on the converging of travel-times:

- Of varying VRP and OFMP
- Only inverting on sections of the model at the time
- Using selected gathers for inversion

This finally produced a model which produced good convergence of travel-times towards picked events (Figure 24), however on the far-offsets of the rightmost airgun shot points (shot numbers above 50) no travel-times where produced. The ray-density analysis shows that the depth of the ray-coverage is even less than for the *modelequal03* (Figure 25).

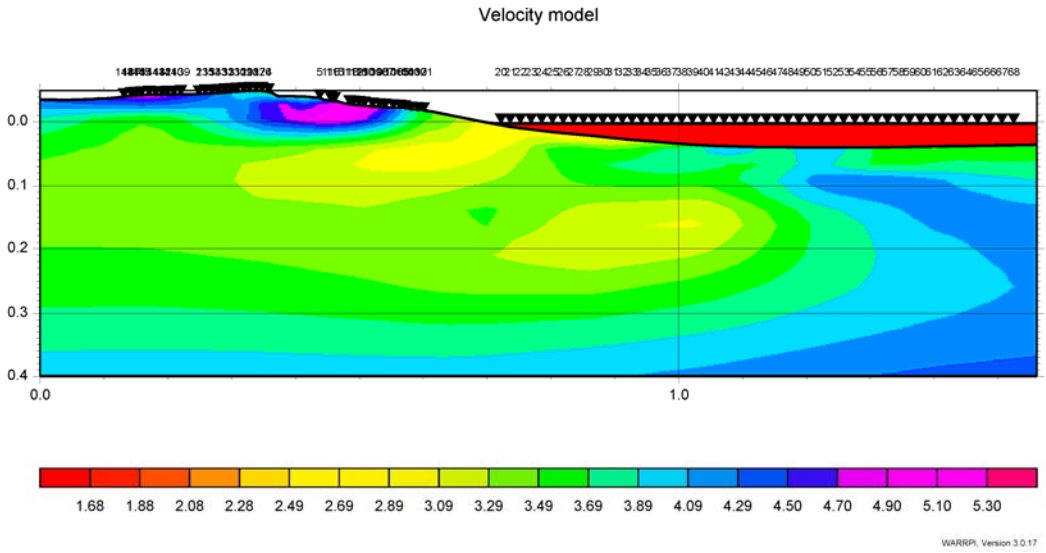

Figure 24. *Modelib21*. Values on colour bar are in km/s. Axes show distance in km.

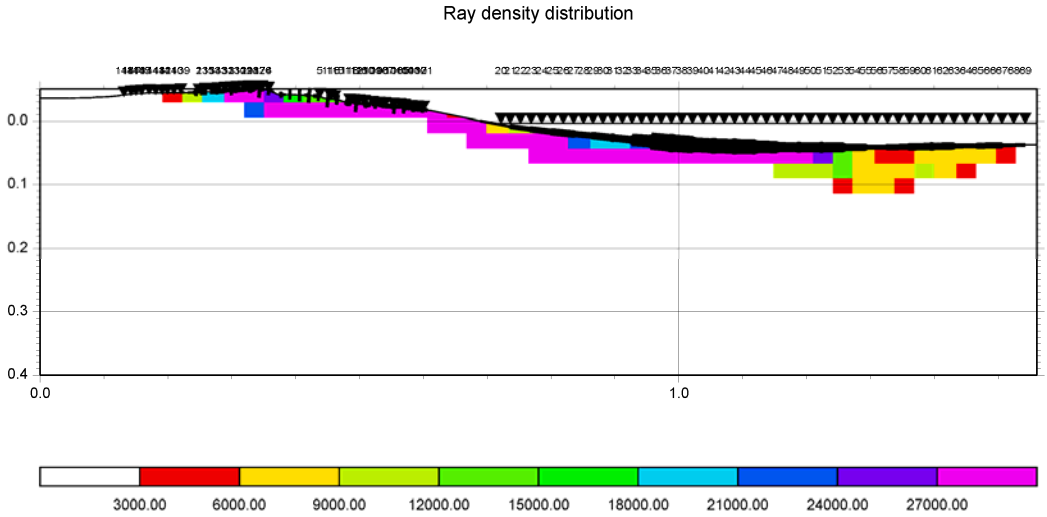

Figure 25. Ray density distribution for *modelib21*: The number of rays that cross the cells divided by the horizontal length of the cell. Axes show distance in km.

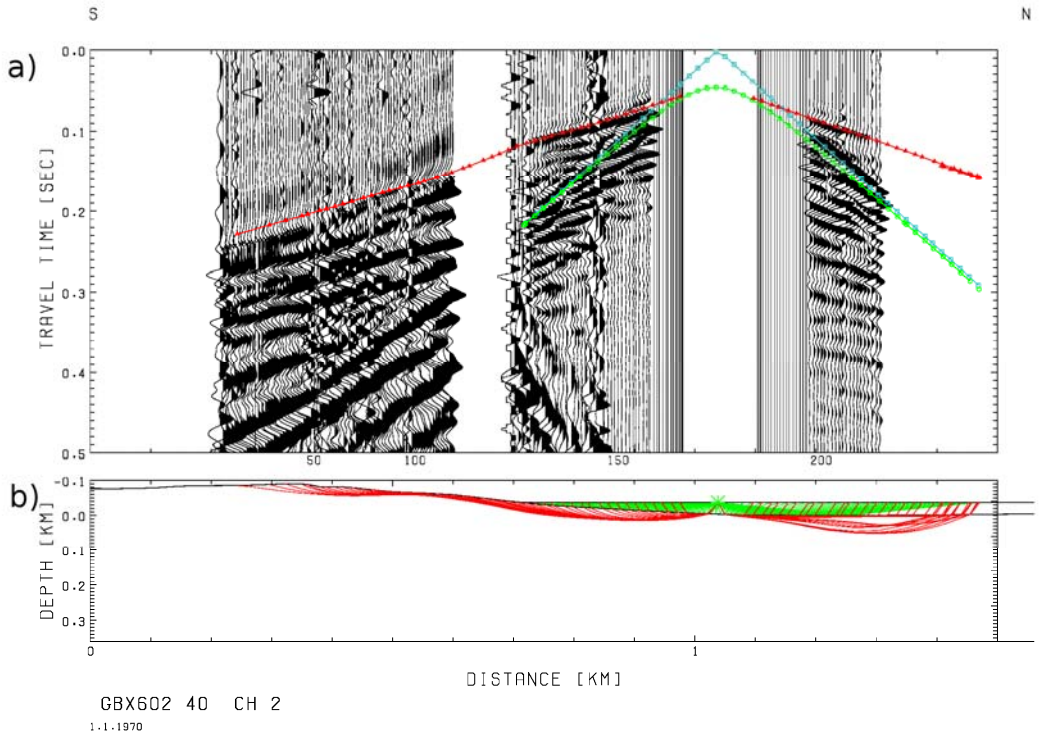

Figure 26. a) Travel times plotted on top of seismic shot gather. b) ray paths for airgun shot point 40. Calculated with *modelib21*. The gather is here plotted with rejected traces muted as illustrated in Figure 9.

The best results were however obtained with a quite different approach. With this approach the final model is obtained in only two steps. The first iteration was with a high VRP value with the purpose of obtaining an initial model, a model that with the least details (coarse model) still produces travel times close to the picked events. Then the next iteration was performed with the lowest possible VRP and OFMP values, the algorithm could handle, thus minimising the effect of the regularisation condition (VRP=0.01 OFMP=0.00001). This procedure gave the best modelling of the expected low-velocity zone and a good convergence of travel times (Figure 27).

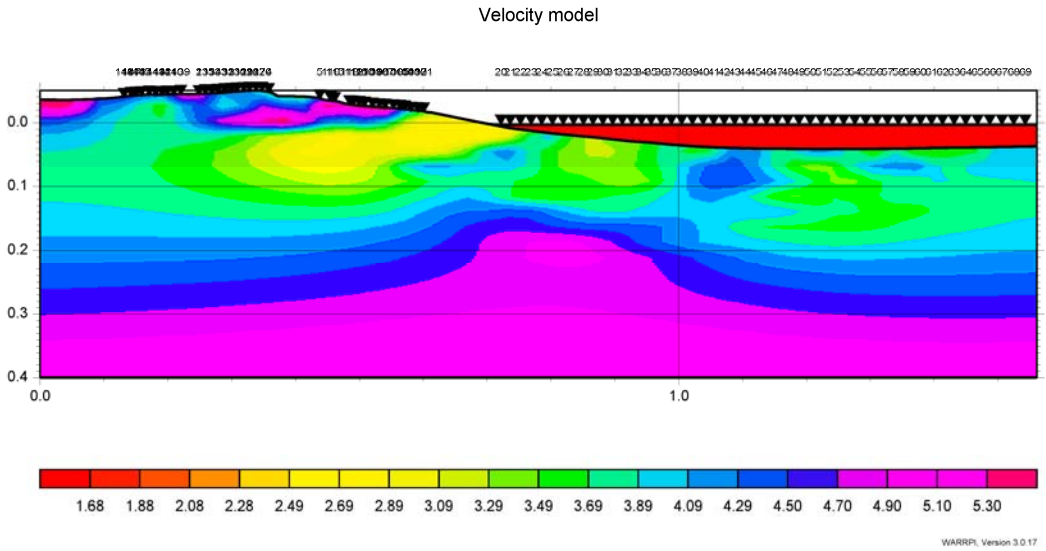

Figure 27. *Modelfinal03*. The final model with fine gridding. Values on colour bar are in km/s. Axes show distance in km.

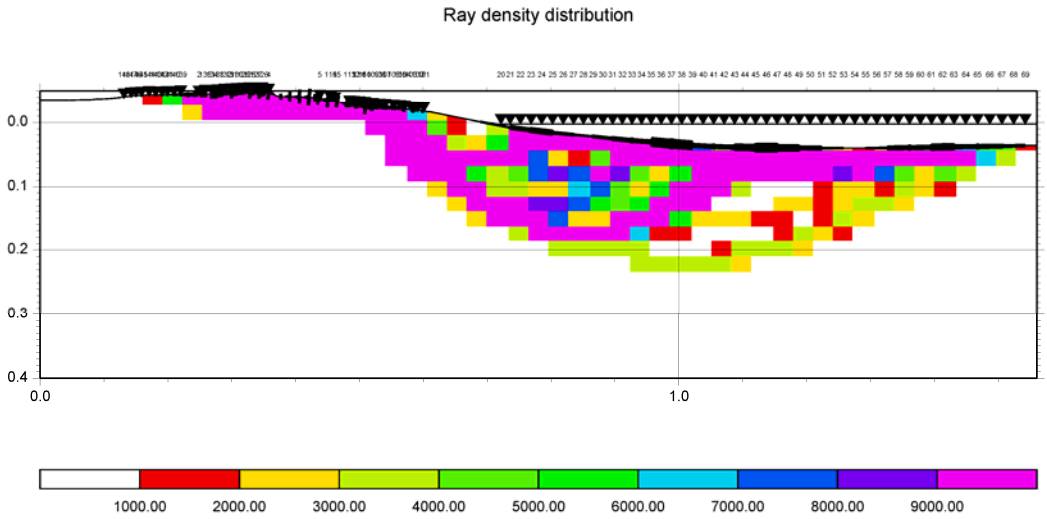

Figure 28. Ray density distribution for the *modelfinal03* (Figure 27).

The reason for that this approach was superior to the more stepwise approaches is most probable due to local-minima's of the error-function. When the iterations are done in small steps, the objective function can be trapped in local-minima's while when doing the inversion in one step, with inversion parameters allowing the inversion algorithm to test a much larger spectrum of solutions, the inversion arrives at a better solution that would have be found otherwise.

Although the converging of the modelled times towards picked events is good, the model does not produce travel times for all gathers, e.g. airgun shot number 66 (Figure 29).

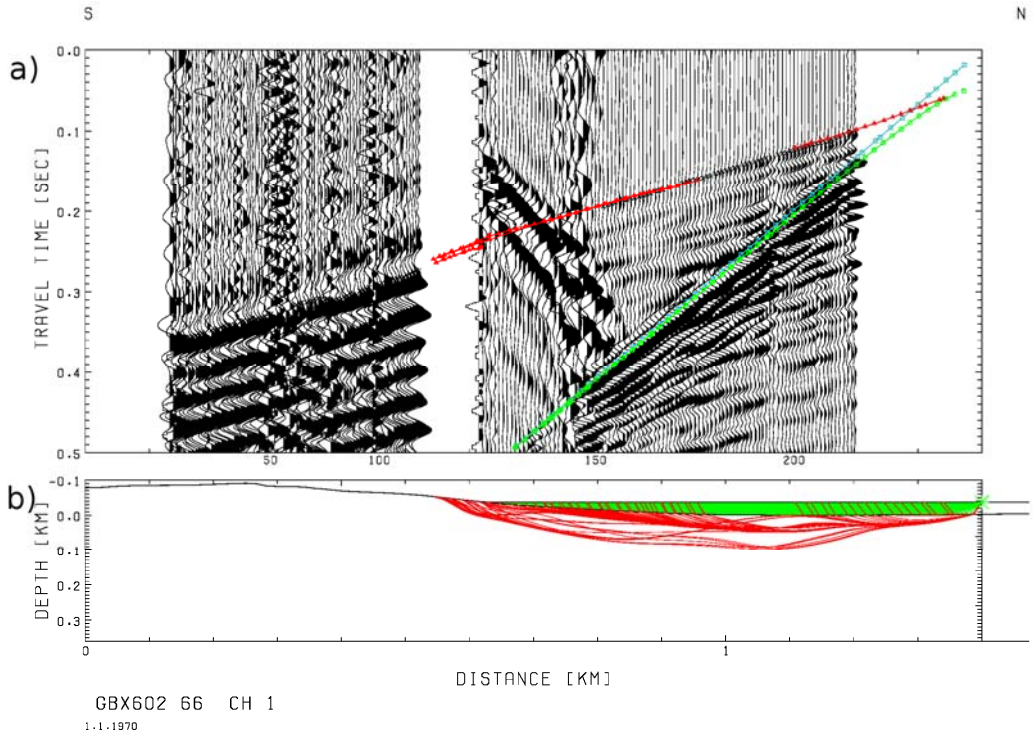

Figure 29. a) Travel times plotted on top of seismic shot gather. b) ray paths for airgun shot point 66. Calculated with *modelfinal03* (See Figure 27).

It turned out that re-sampling the velocity grid, of the *modelfinal03*, from the initial 50x20 to 20x10 grids resulted in travel times for most of the picked events (*modelfinal04*, Figure 30).

The travel times modelled by *modelfinal04* also have a better convergence towards picked travel times. The RMS for *modelfinal04* is 0.0086 (calculated difference between picked travel times and modelled travel times) relative to 0.0168 for *modelfinal03*.

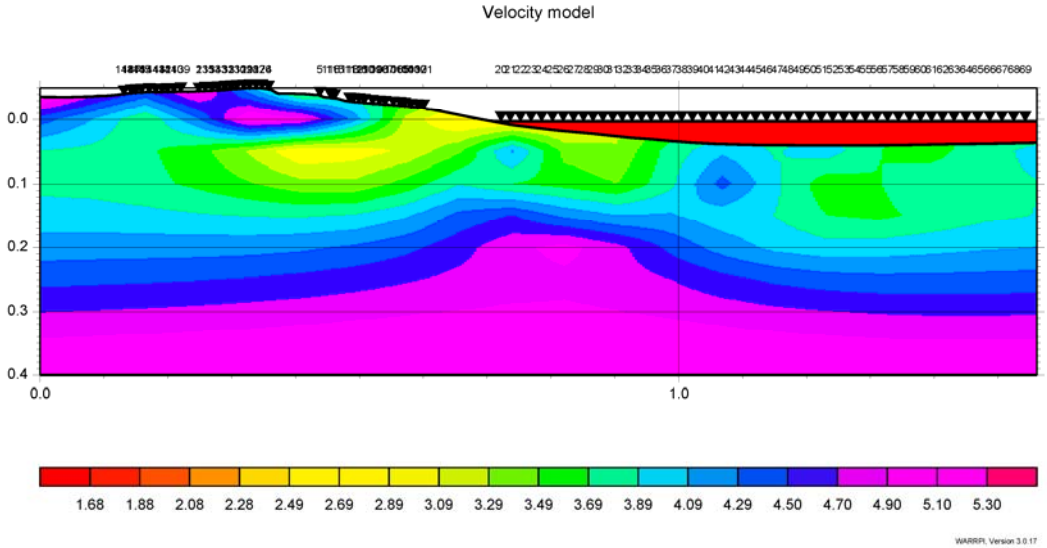

Figure 30. *Modelfinal04*. The velocity grid of *modelfinal03* re-sampled from 50x20 to 20x10. Values on colour bar are in km/s. Axes show distance in km.

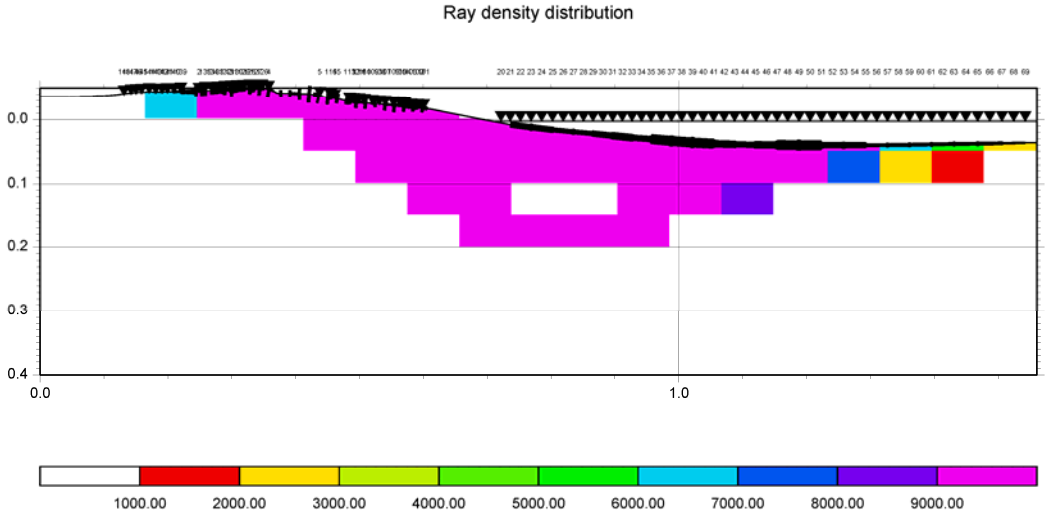

Figure 31. Ray density distribution for *modelfinal04* (See Figure 30).

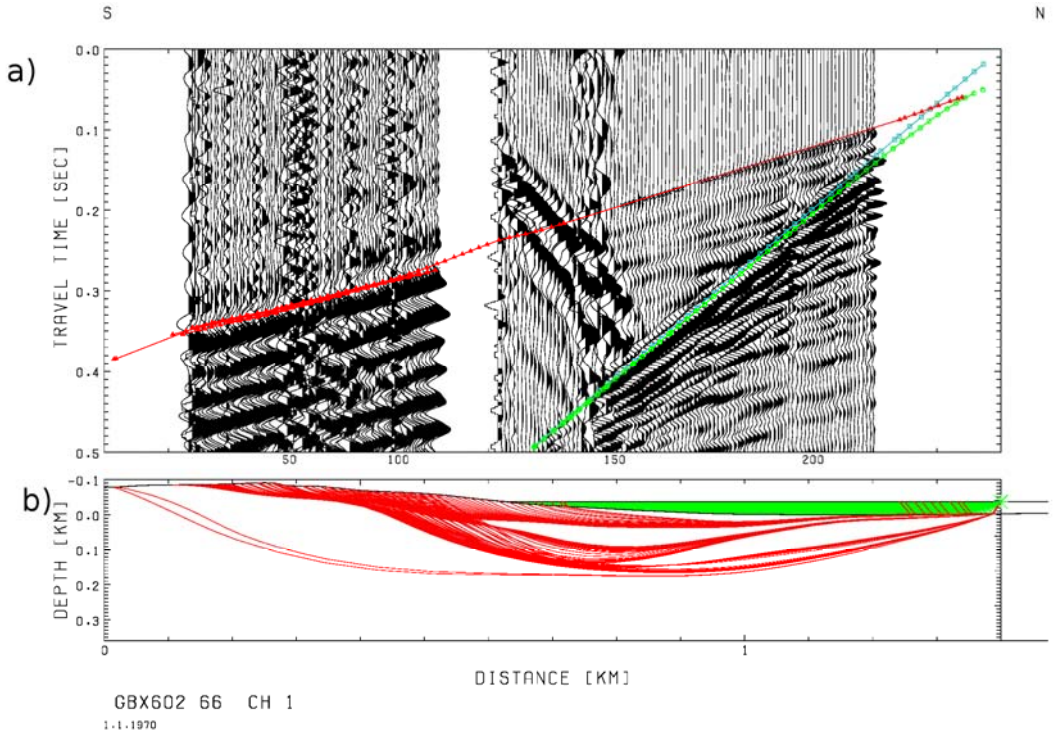

Figure 32. a) Travel times plotted on top of seismic shot gather. b) ray paths for airgun shot point 66. Calculated with *modelfinal04* (See Figure 30).

Based on this result the initial grid spacing was reconsidered. It was now tested whether a starting model with 20x10 grid points, inverted in two steps as above, would produce better results. This was however not so and several different grids were tested on the inversion by two steps as above without better results.

So although the coarser grid produces a more consistent model, the initially finer velocity grid was necessary to arrive at the solution.

3.3 Error estimates

Uncertainties can be divided into dependent and independent uncertainties.

The data used for the inversion have densely sampled shot points and station positions. The solution is obtained while trying to satisfy all data points simultaneously. Errors imposed by the independent uncertainties will to a large extent be averaged out. Therefore independent uncertainties will have little quantitative effect on the results but will be more likely to have a qualitative effect, which means that while the magnitude of the numerical values of the velocity distribution will not be affected very much, the delineation of the velocity distribution might be less well defined. The main cause of independent uncertainties is from uncertainties in picking of events

Dependent uncertainties can on the other hand have a large effect on the resulting velocity distribution. In that case the errors will not be averaged out but will on the contrary be enhanced. Examples of dependent uncertainties are: position errors and uncertainties in the zero times of gathers.

3.3.1 Independent uncertainties

The effect of independent uncertainties was quantified by imposing a random error of ±5 ms (Figure 33) on all picked events (Figure 34) and inverting with same parameters as used for the *modelfinal03*. The resulting model is named *modelfer03* (Figure 35) and the model with re-sampled velocity grid is named *modelfer04* (Figure 36).

The models show the same general velocity distribution (locations for high/low velocity zones) as the *modelfinal03* (Figure 27) and *modelfinal04* (Figure 30). The difference in velocities is less than ±4% for the *modelfer03* (Figure 37) and even lesser for the *modelfer04* (Figure 38).

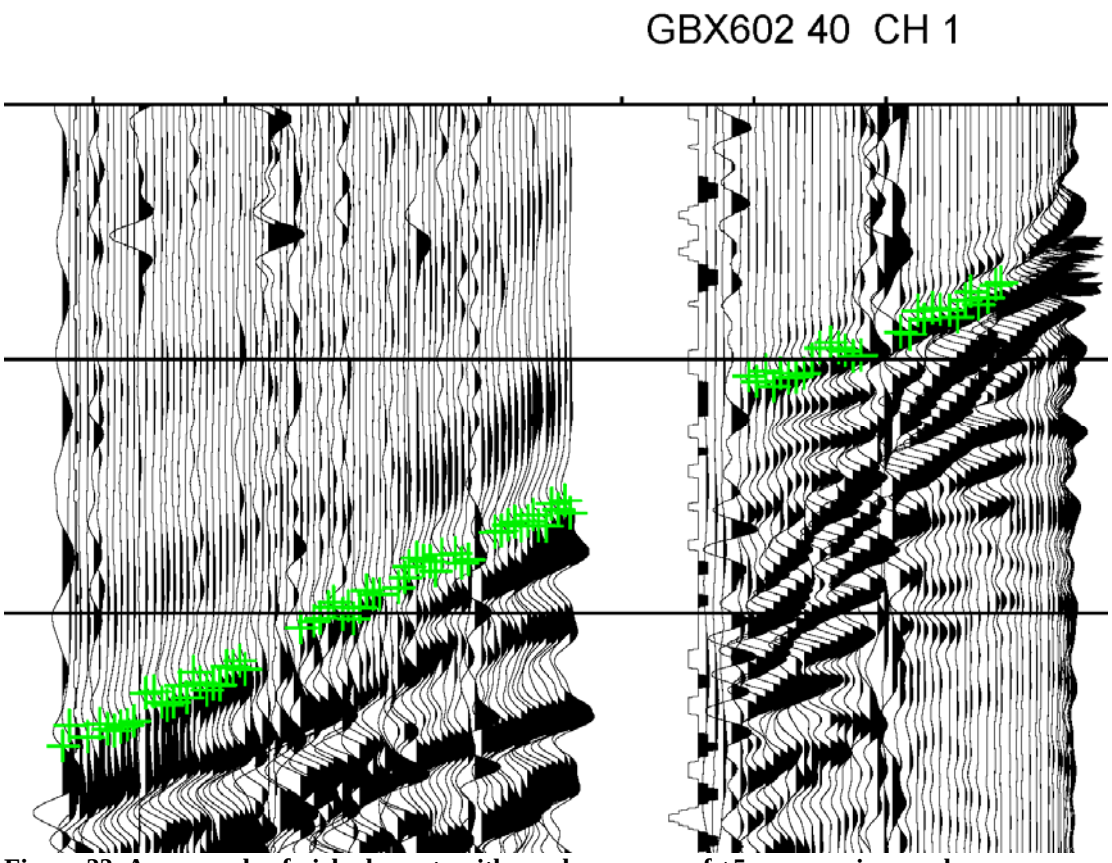

Figure 33. An example of picked events with random errors of ±5 ms superimposed.

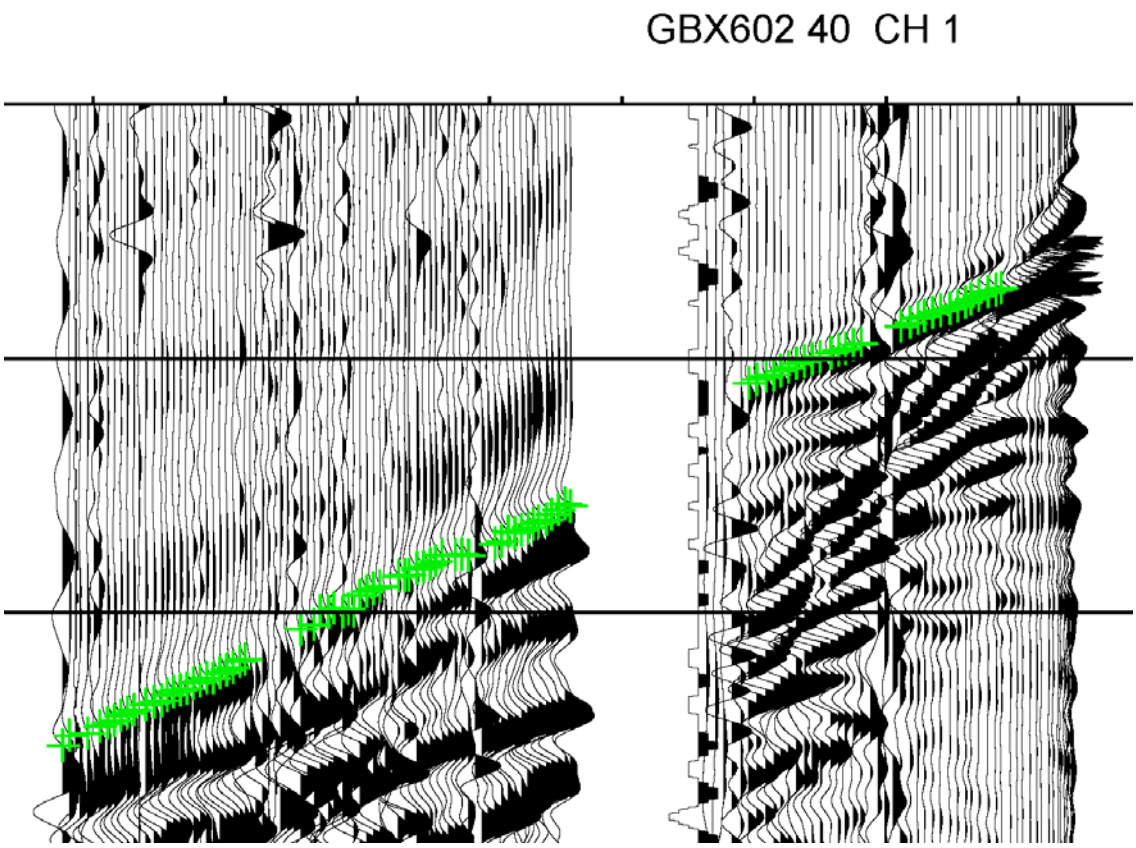

Figure 34. The same gather as in Figure 33 before superimposing the random errors.

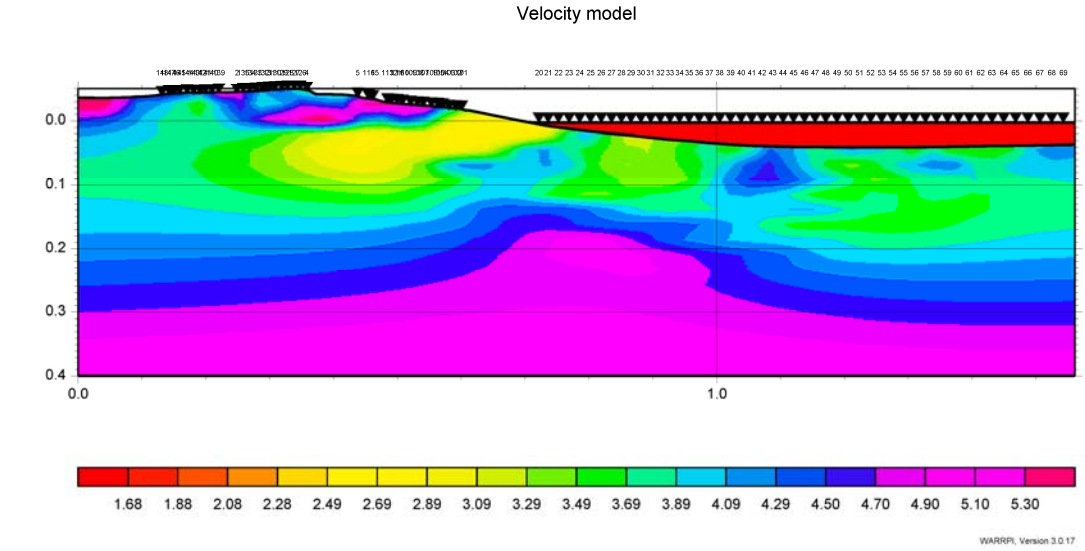

Figure 35. *Modelre03*. To be compared with *modelfinal03* in (Figure 27).

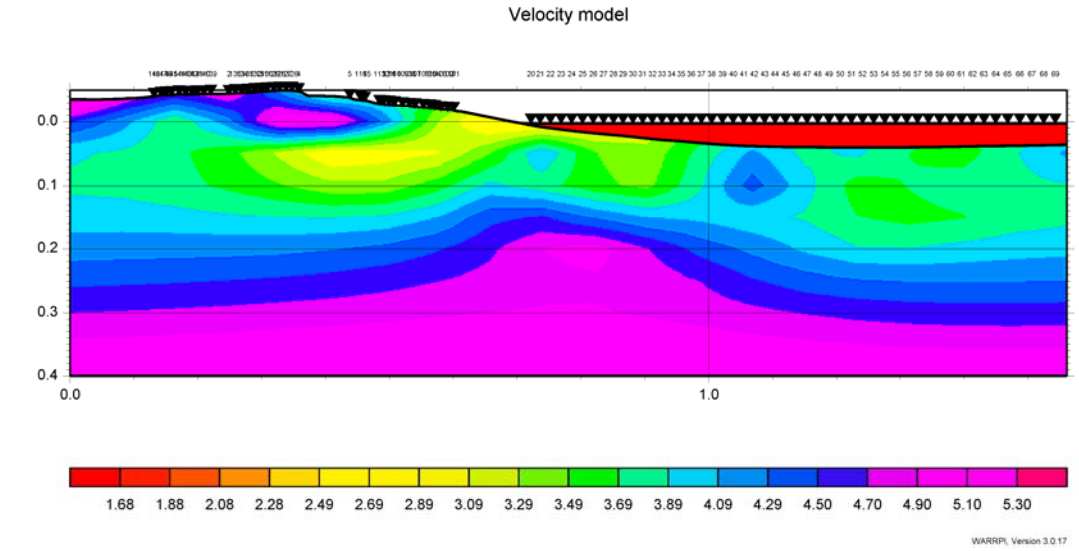

Figure 36. *Modelre04*. To be compared with *modelfinal04* (Figure 30).

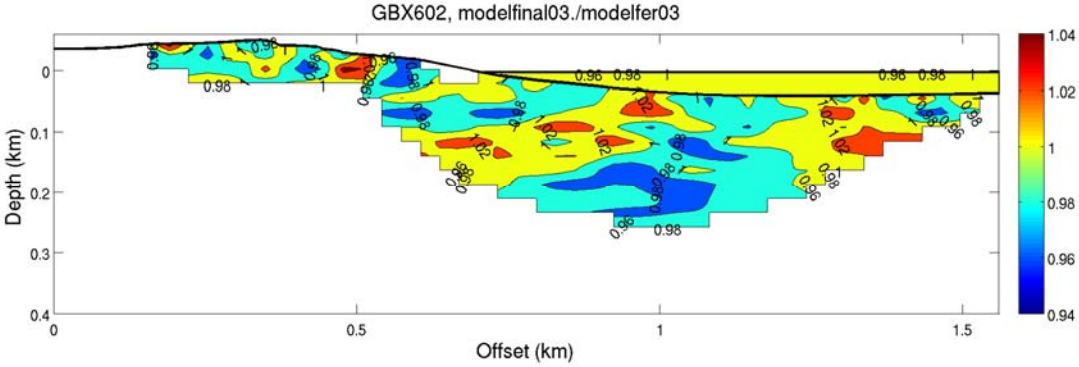

Figure 37. The *modelfinal03*/*modelfer03* ratio.

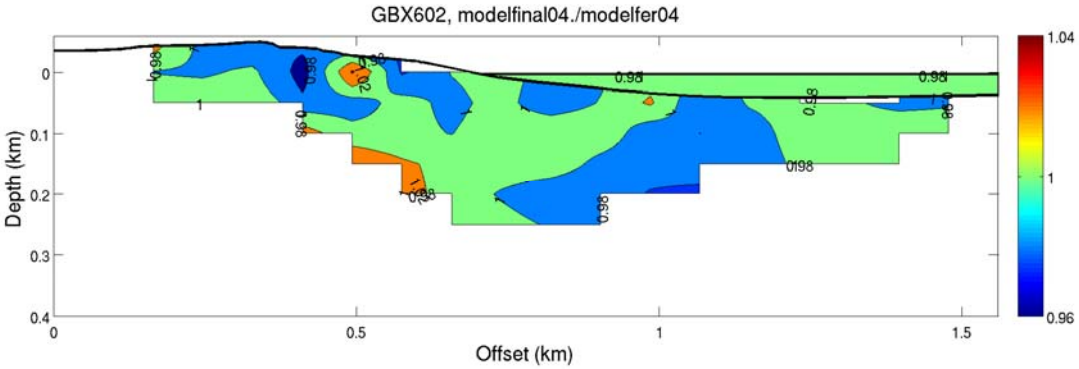

Figure 38. The *modelfinal04*/*modelfer04* ratio.

3.3.2 Dependent uncertainties

The dependent uncertainties will be divided into the time domain and the spatial domain.

3.3.2.1 Time domain

The most obvious dependent uncertainty in the time domain is the establishing of zero time for the gathers. The effect of 5 ms time-shift downwards was tested (Figure 39). The resulting model is inverted with same parameters as for the *modelfinal03* and is named *modelftsh03* (Figure 40). The re-sampled model is named *modelftsh04* (Figure 41). The location of low/high velocity zones is preserved while the very shallow velocities are significantly affected. The deeper velocities are however within %5 from the original models (Figure 42 and Figure 43)

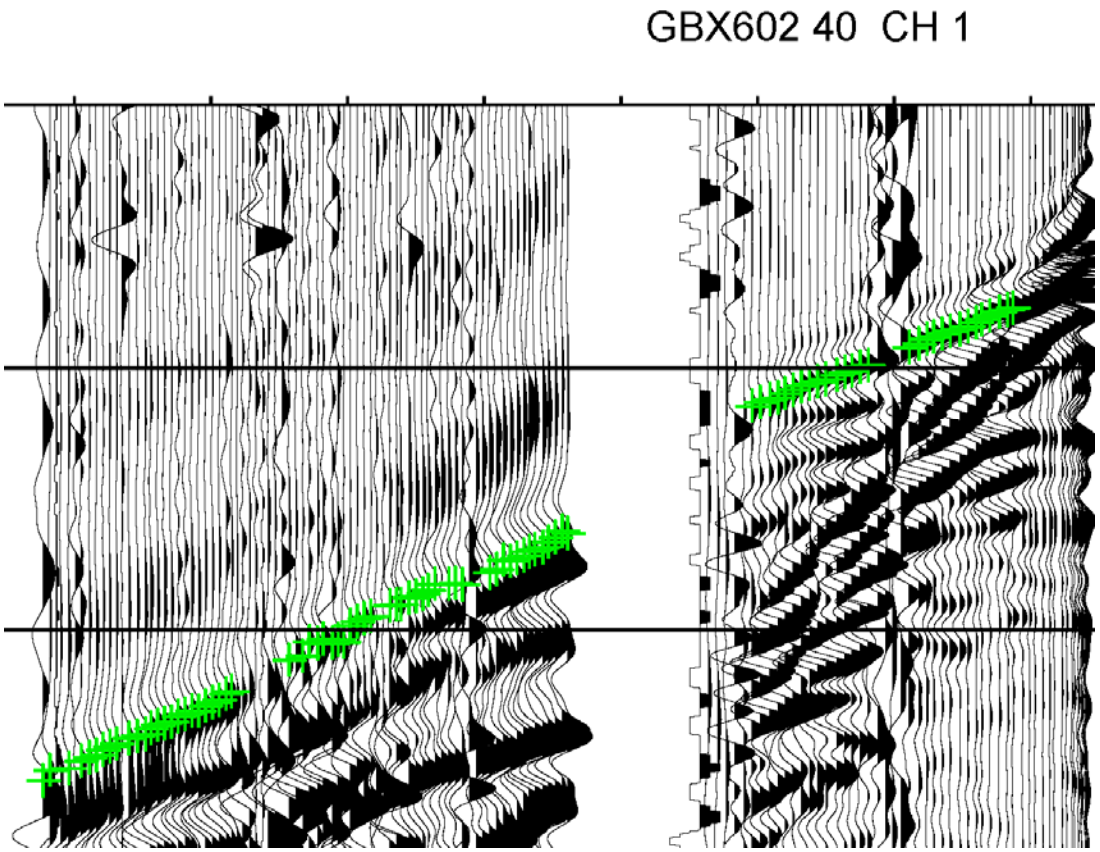

Figure 39. Timeshift 5 ms downards relativ to original pickings shown in Figure 34.

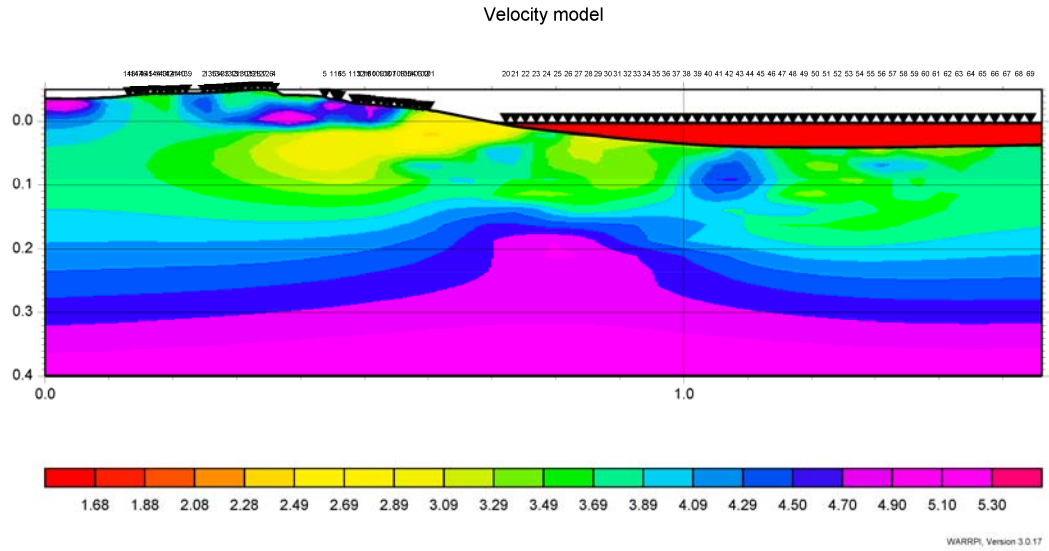

Figure 40. *Modelftsh03*. To be compared with *modelfinal03* (Figure 27). Values on colour bar are in km/s. Axes show distance in km.

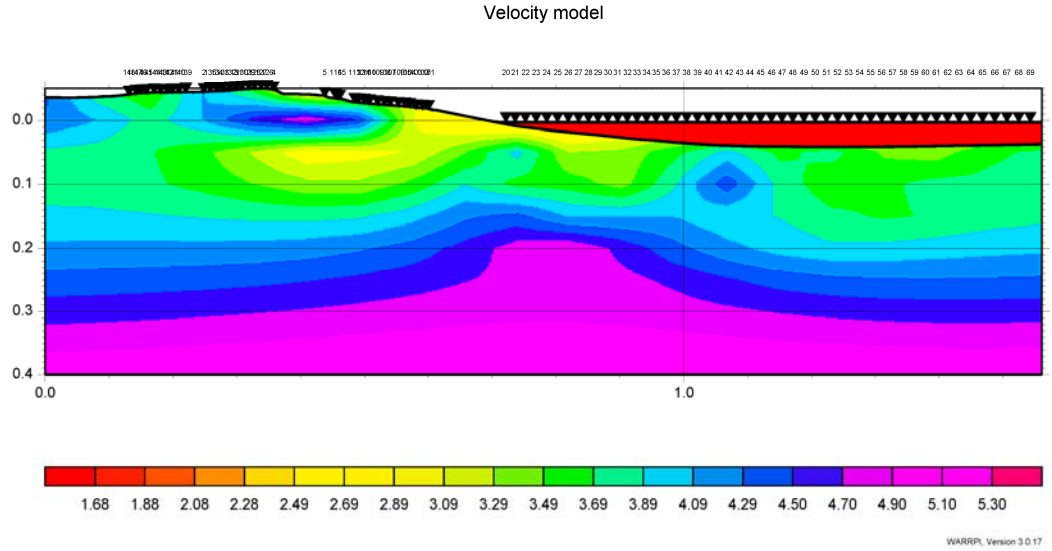

Figure 41. *Modelftsh04*. To be compared with *modelfinal04* (Figure 30). Values on colour bar are in km/s. Axes show distance in km.

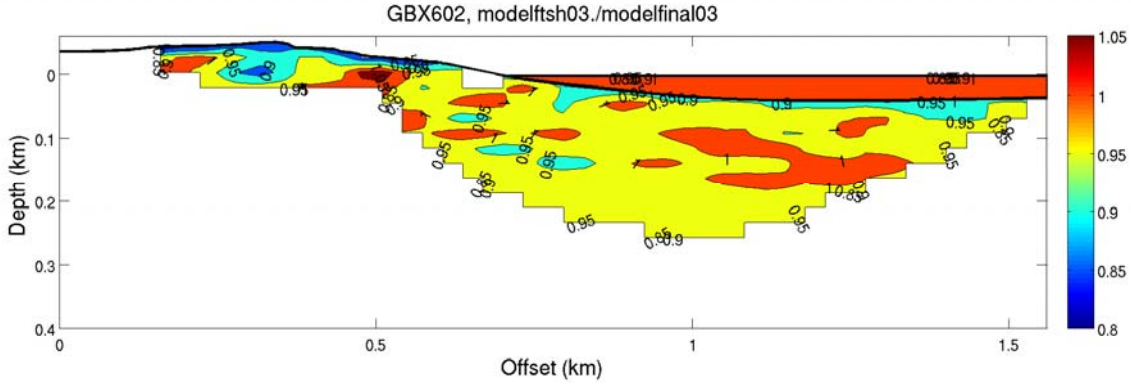

Figure 42. The *modelftsh03*/*modelfinal03* ratio.

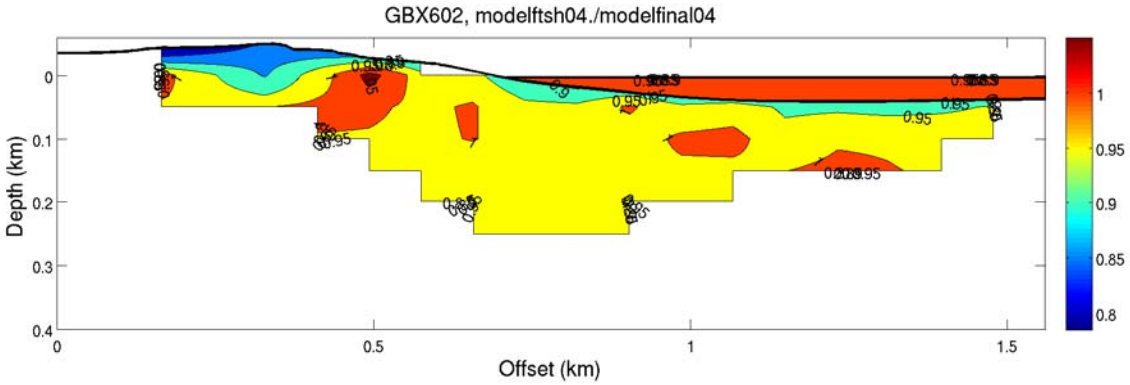

Figure 43. The *modelftsh04*/*modelfinal04* ratio.

3.3.2.2 Spatial domain

Since the uncertainties relating to the station interval are relatively small they will be disregarded. The position of the geophone layout will thus be considered as one object. Similarly the position of the streamer is considered as one object.

The positions of the geophone layout are with high precisions while the streamer layout has less precision.

In chapter 2.4.2 on the positioning of the streamer it is shown that there is a difference whether the positioning is based on the jack-up rig and tugboat position or based on the shot point positions. If the streamer positions where from jack-up rig and tugboat only, the streamer would be placed ~5 m further to the north than if it is positioned based on shot point positions.

The effect of shifting the streamer 20 m to the north was tested (Figure 44). A 20 m shifting of the streamer was chosen in order to make a somewhat larger shifting than the 5 m and thus see to what extent the low-velocity zone between the geophones and streamer is affected. The positioning of the streamer is relative to the airgun shot points so the airgun shot points where shifted the same amount.

The resulting model was inverted with same parameters as for the *modelfinal03* and is named *modelfsh03* (Figure 45) and the re-sampled model is named *modelfsh04* (Figure 47). As expected, the largest effect is on the section between the geophone and streamer layout. In this section the very shallow velocities are 20% higher than in the original model (Figure 47 and Figure 48). Otherwise the velocities are within ±10% from the original models. So even with a large shifting of the streamer towards the north the velocities of the low-velocity zone between the geophones and streamer are preserved.

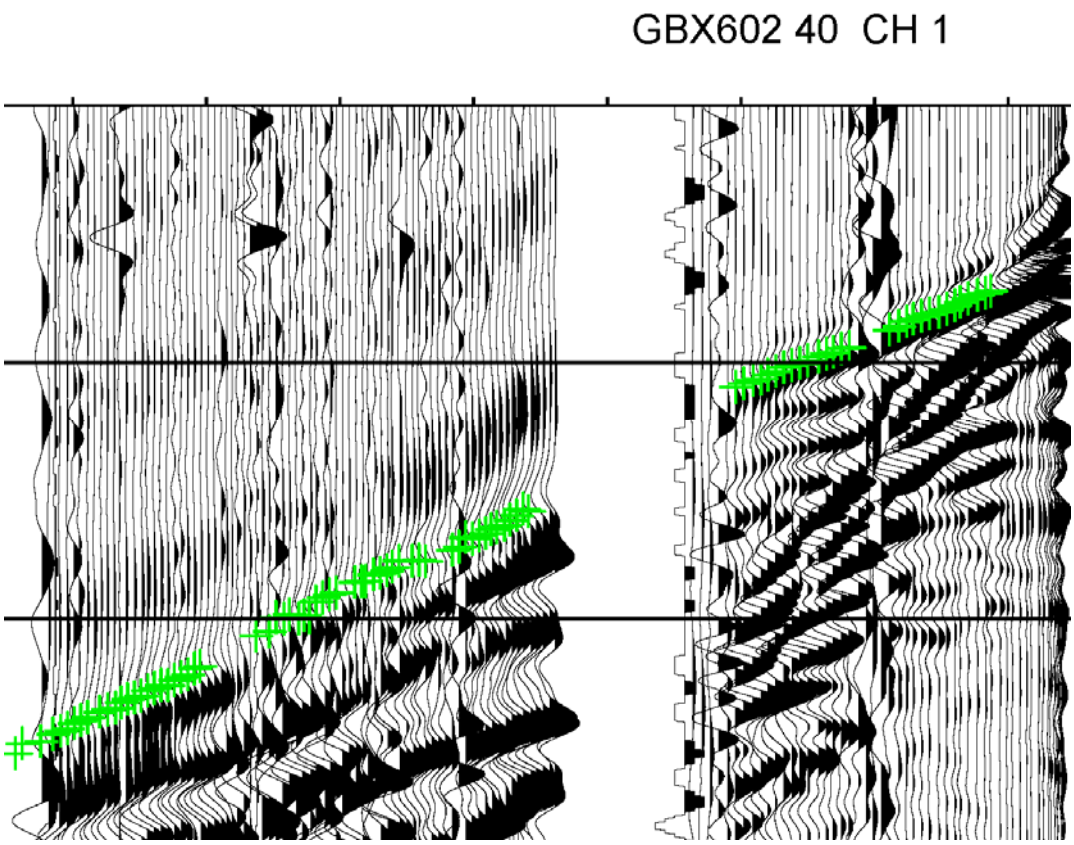

Figure 44. Shifting the streamer and airgun shot positions to the north. The offset between the geophones and streamer is increased. Original gather is shown in Figure 34.

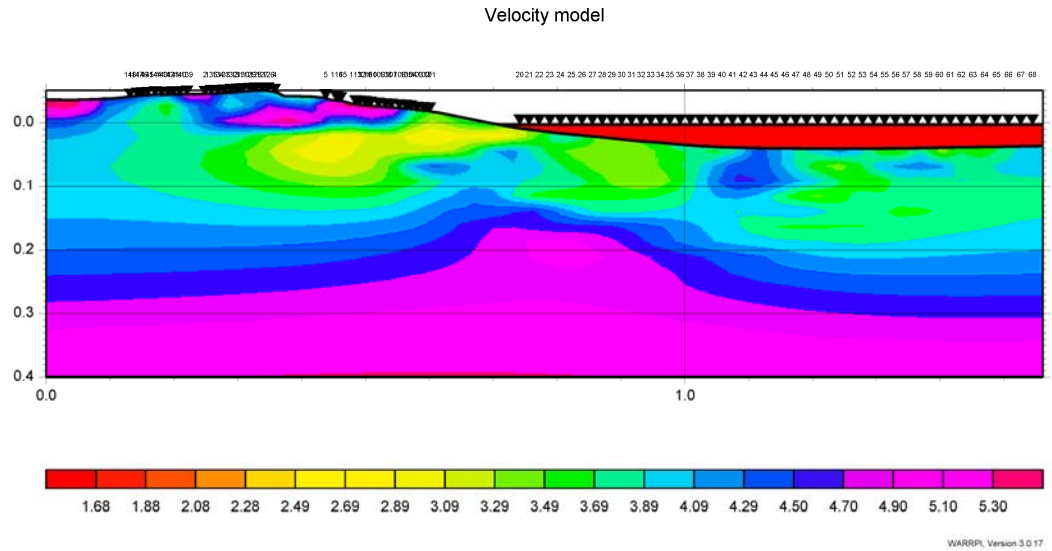

Figure 45 *Modelftsh03*. To be compared with *modelfinal03* (Figure 27). Values on colour bar are in km/s. Axes show distance in km.

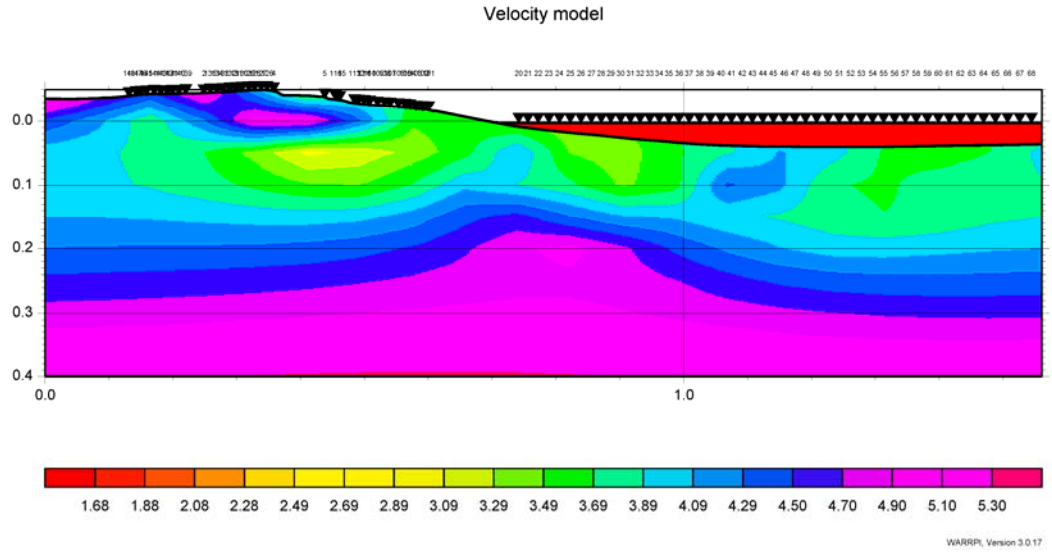

Figure 46 *Modelftsh04*. To be compared with *modelfinal04* (Figure 30). Values on colour bar are in km/s. Axes show distance in km.

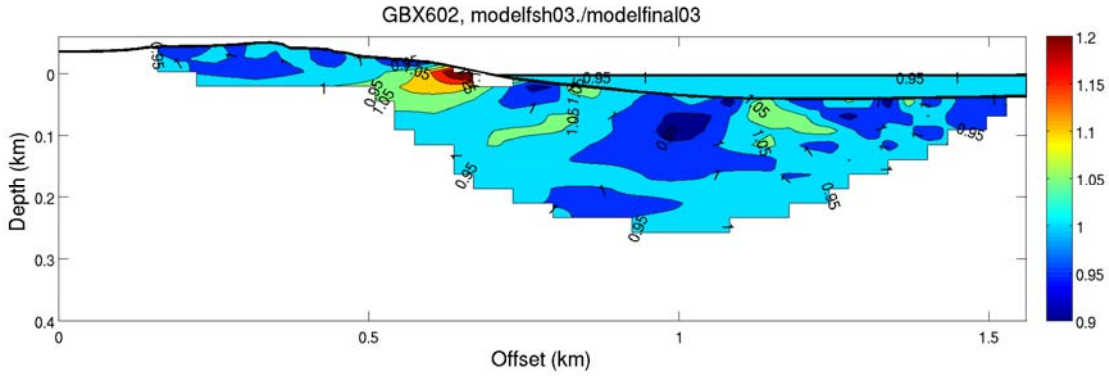

Figure 47 *modelfsh03*/*modelfinal03* ratio

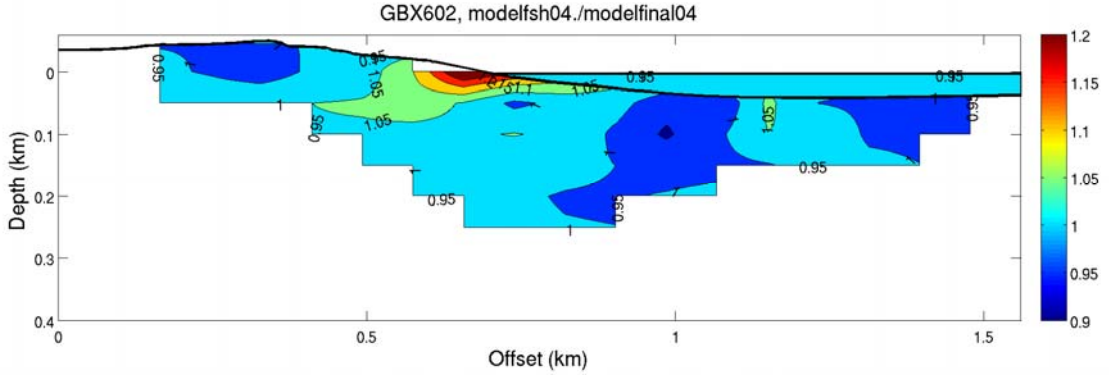

Figure 48 *modelfsh04*/*modelfinal04* ratio

3.3.3 Root Mean Square

RMS values for all models are listed in Table 2 and Table 3.

Model	RMS
modelfinal03	0,017
modelftsh03	0,013
modelfsh03	0,034
modelftosh03	0,030
modelfer03	0,014

Table 2

Model	RMS
modelfinal04	0,0086
modelftsh04	0,0069
modelfsh04	0,0118
modelftosh04	0,0078
modelfer04	0,0091

Table 3

3.4 Correlation to geological information

The correlation to known geology in the area serves two purposes. On one hand the velocity distribution establishes velocity properties of geological structures in the area and on the other hand it gives an indication of the extent to which it is possible to interpret geological structures directly from the modelled profile.

3.4.1 Correlation to the surface mapping of the Glyvursnes area and to the lithology in the Glyvursnes-1 composite well log

As a part of the SeiFaBa project, Simon Passey performed a geological survey of the area surrounding the Glyvursnes-1 well in order to establish the stratigraphy of the younger rock units that were not encountered in the well and to evaluate any structural features in the area (Passey 2005).

The lowest part of the mapped stratigraphic sequence intersects with the modelled profile. Based on the expected seismic properties of the mapped units, a few markers (Figure 49 A, B and C) are defined to be used for the correlation to the modelled profile.

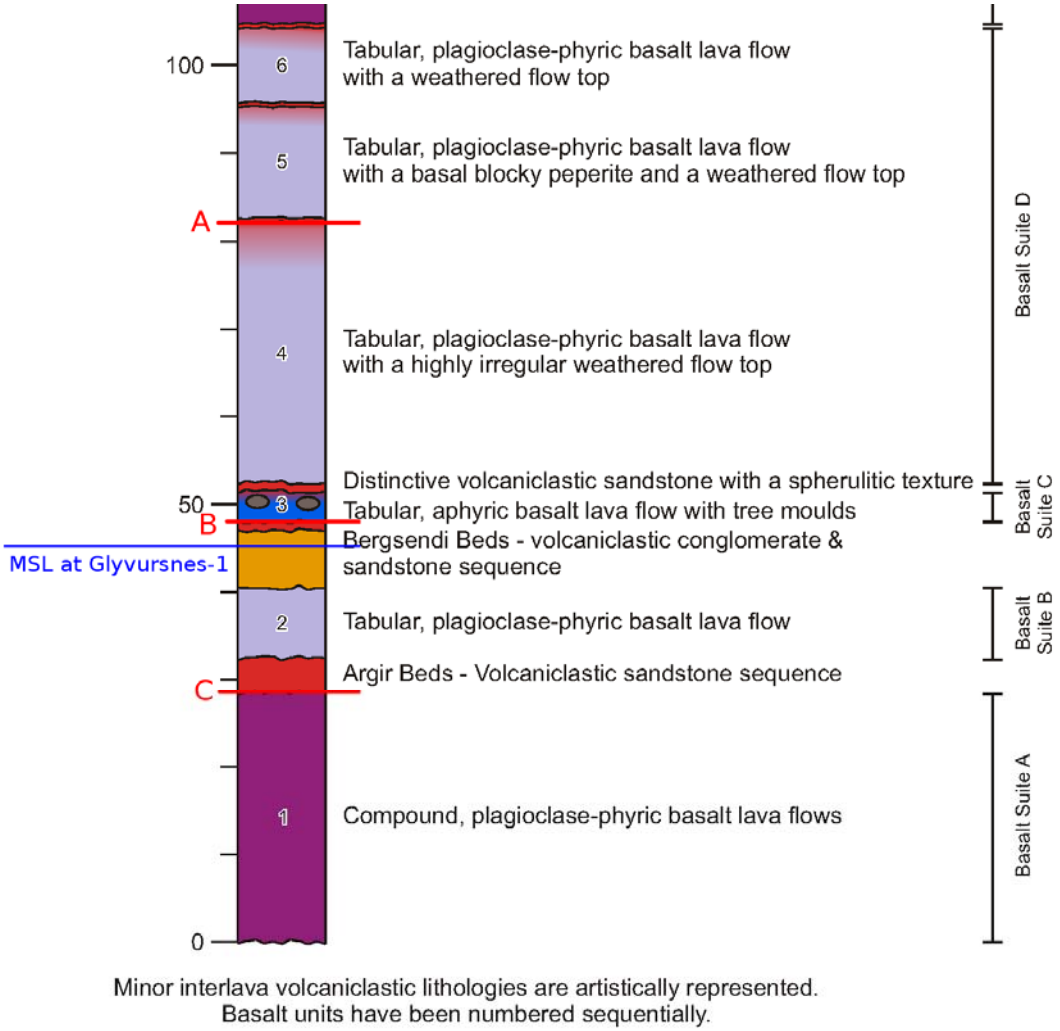

Figure 49. Stratigraphic sequence modified from Passey (2005). Blue horizontal line is the approximate location of the mean sea level for the stratigrapy at the Glyvursnes-1 location. The red lines marked A, B and C are used for extrapolation onto the velocity profile.

The section between A and B consists mainly of a 25-35 m thick tabular basalt flow and is thus expected to be a high-velocity zone. The section between B and C consists mainly of ~4 m thick sandstone, a ~8 m thick tabular basalt flow and a 9-16 m thick volcaniclastic sequence and is thus expected to be a low-velocity zone.

For a detailed description of the stratigraphic sequence I refer to the original report by Passey (2005).

The markers were extrapolated onto the modelled profile by the following procedure: First the geological map from Passey (2005) was folded onto the topography and bathymetry of the area in question. Then surfaces with strike and dip corresponding to the mapping of Passey were fitted to comply with the appropriate interfaces (Figure 50).

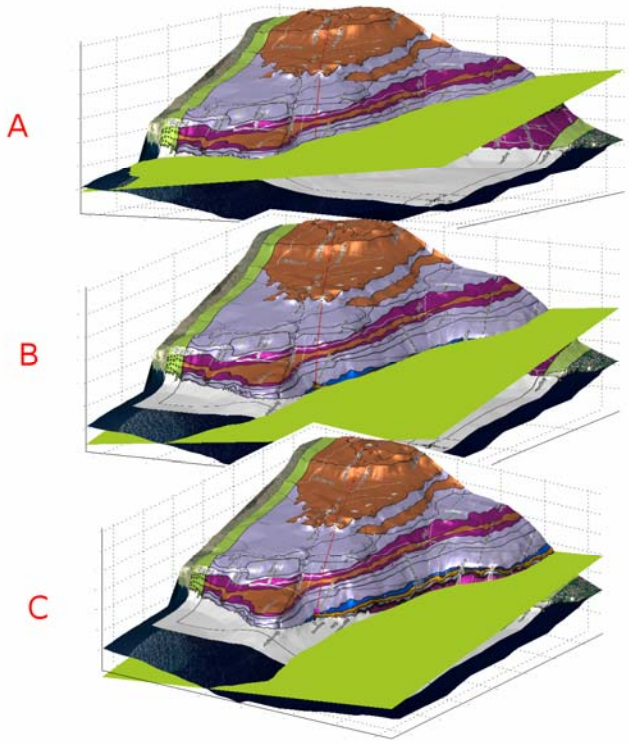

Figure 50 The markers A, B and C from Figure 49 extrapolated as flat surfaces.

Using this strike and dip, the surface for marker A fits well to the location of the mapped top of basalt-flow number 4 for the whole map. Similarly the surface for marker B fits well to the location of the mapped top of the volcaniclastic sequence. But the surface that corresponds to the base of Argir Beds does have a less well defined fit.

The interpreted well log (Waagstein and Andersen 2003) was used to establish the depth of the surface for marker C. By this approach the surface was found to match the location of the Argir Beds as indicated on Figure 5 in the "Geology of Glyvursnes" (Passey 2005)

Figure 51 shows that the section between marker A and B does correlate to a well defined high-velocity section of the modelled profile. And that the section between marker B and C correlates to a low-velocity section of the modelled profile. The velocity distribution complies well with the dip of the extrapolated markers.

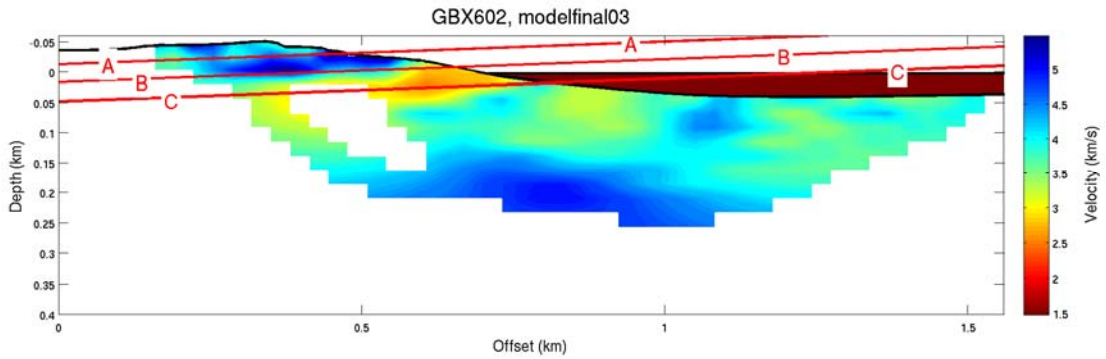

Figure 51 shows the velocity profile with the extrapolated markers annotated. The sections of the model with little ray-coverage have been removed (white).

Where marker C crosses the seabed coincides with the base of a low-velocity zone while farther to the left the low-velocity zone extends below marker C.

Based on the interpreted composite well log more markers to be correlated to the velocity profile were defined. For a detailed description of the well log I refer to the *Well Completion Report* (Waagstein and Andersen 2003).

Some markers related to thick massive lava cores where defined (Figure 52, Table 4).

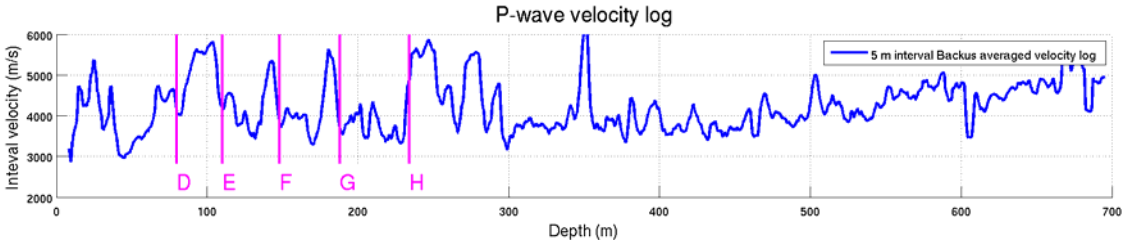

Figure 52. P-wave velocity log. Definition of markers to extrapolate onto the modelled profile.

Marker	Depth (m)		Log velocity (km/s)
B	12	Top Bergsendi Beds	
C	44	Base Argir Beds	
D	84	Top of a ~25 m thick massive lava core	
E	110	base of a ~25 m thick massive lava core	~5.5 km/s
F	148	Base of a ~15 m thick massive lava core	~5.5 km/s
G	188	Base of a ~15 m thick massive lava core	~5.5 km/s
H	232	Top of a ~20 m thick massive lava core	~5.5 km/s

Table 4 shows the markers as they are defined in this project.

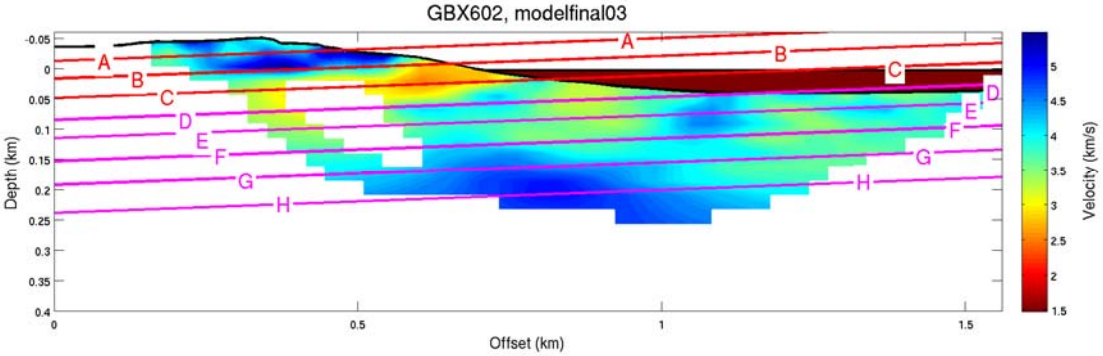

Figure 53 Shows the velocity profile (*modelfinal03*) with the extrapolated markers annotated. The sections of the model with low ray-coverage have been removed.

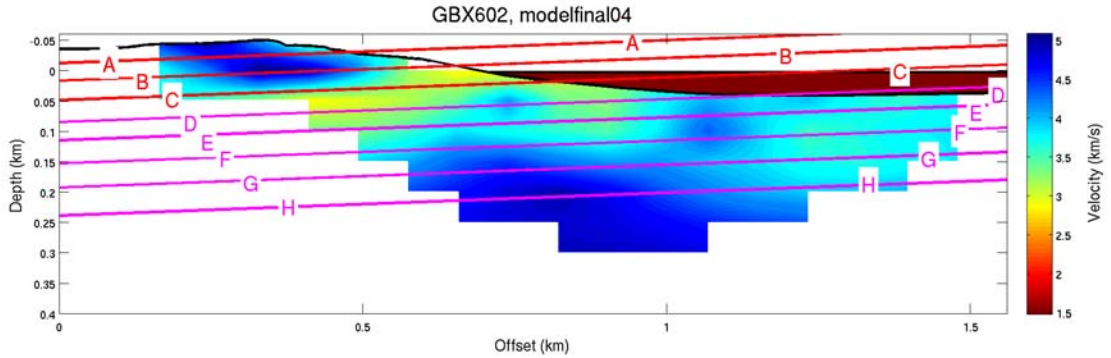

Figure 54. Shows the velocity profile (*modelfinal04*) with the extrapolated markers annotated. The sections of the model with low ray-coverage have been removed (white).

While there was good consistency between the velocity model and the surface geological mapping by Passey (2005) presented above, there is mush less immediate conformity between the deeper markers and the velocity model.

All of the markers do at some point coincide with expected high velocities zones but the zones do not have the anticipated horizontal extension.

The missing horizontal spreading of the high-velocity zones could be an artefact from the modelling method. This would be attributed to ray-paths being captured in certain areas of the model. Figure 55 and Figure 56 show the resulting model could be consistent with a thick high-velocity zone in the D-E interval and with the high velocity zones in F and G. Due to the capturing of rays in certain positions most of the layer has relatively little coverage and the area in the layer with the expected high velocities do actually have the highest concentration of rays.

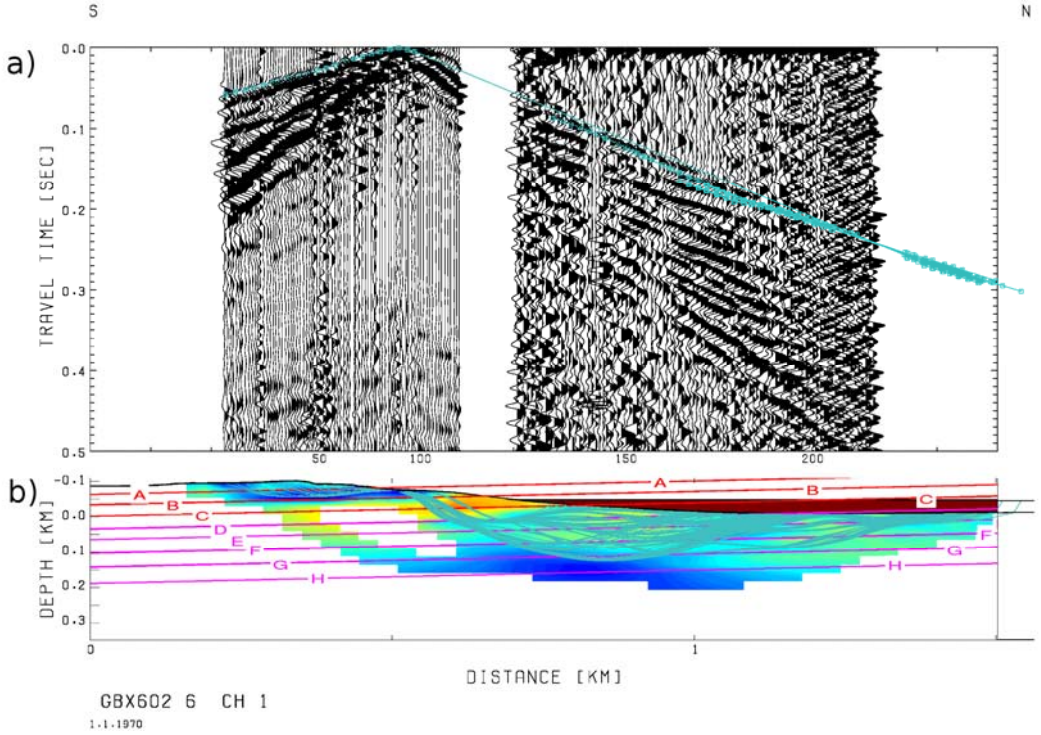

Figure 55 a) Travel times plotted on top of seismic shot gather. b) Ray paths for dynamite shot point 6 plotted on top of velocity model. Calculated with *modelfinal03*.

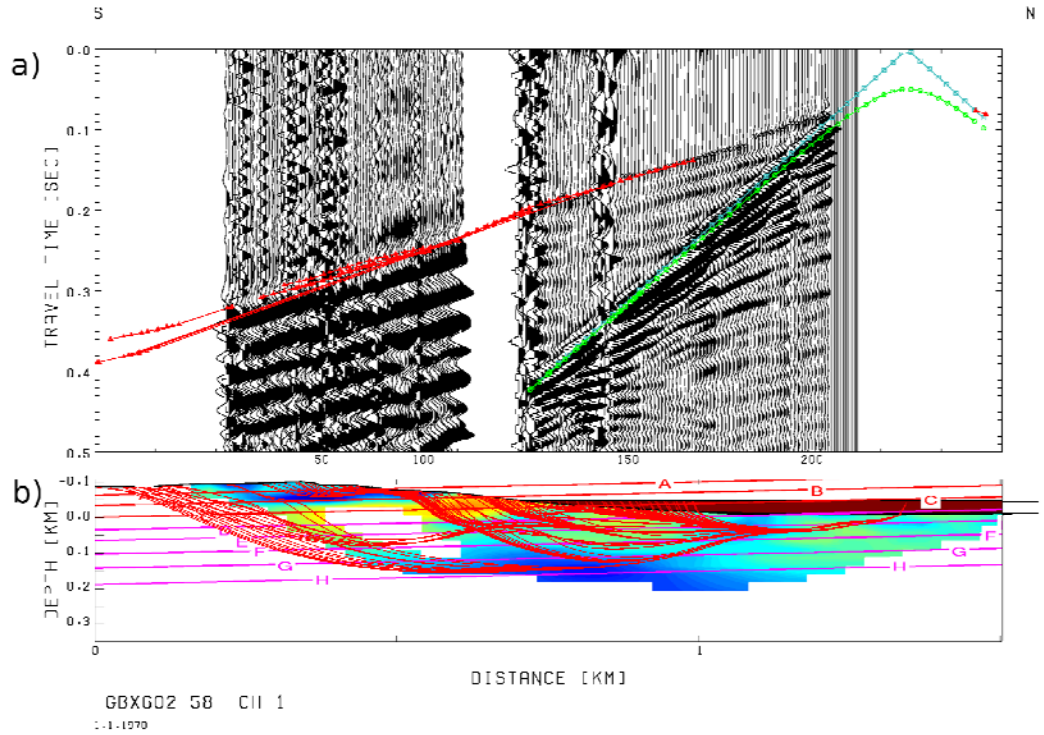

Figure 56 a) Travel times plotted on top of seismic shot gather. b) Ray paths for airgun shot point 58 plotted on top of velocity model. Calculated with *modelfinal03*.

The ray paths in Figure 55 and Figure 56 express very well the nature of the total ray density distribution as illustrated in Figure 28. So the unequally distributed horizontal velocity spreading can be due to ray coverage but it can also be an expression for actual velocity variations.

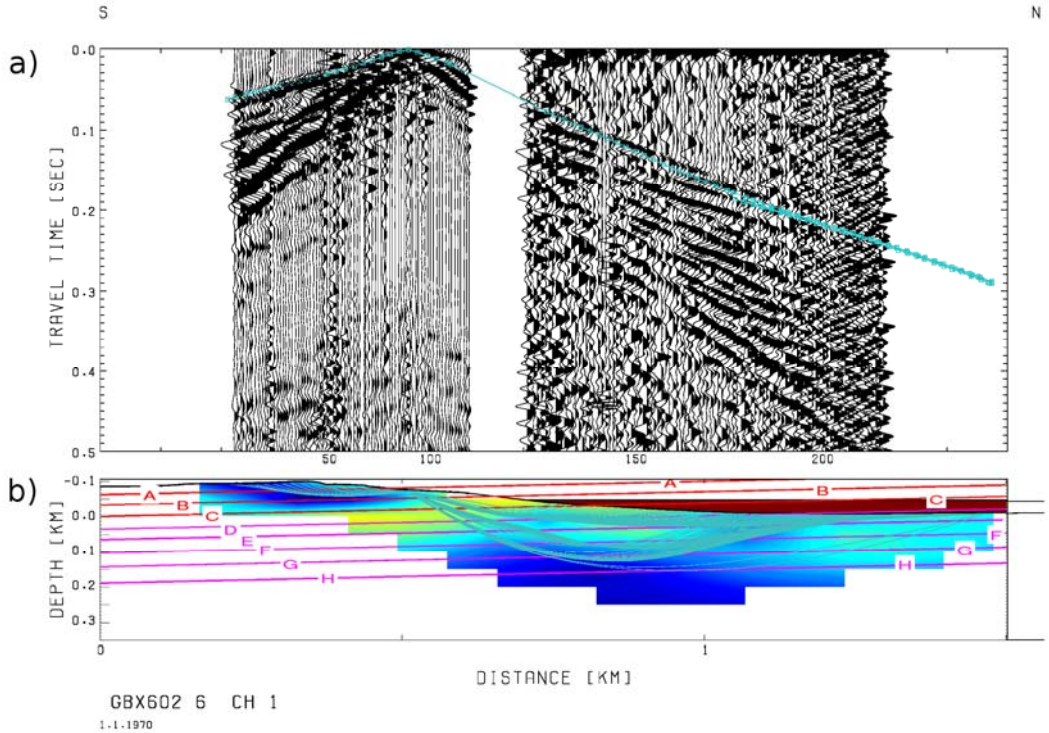

Figure 57 a) Travel times plotted on top of seismic shot gather. b) Ray paths for dynamite shot point 6 plotted on top of velocity model. Calculated with *modelfinal04*.

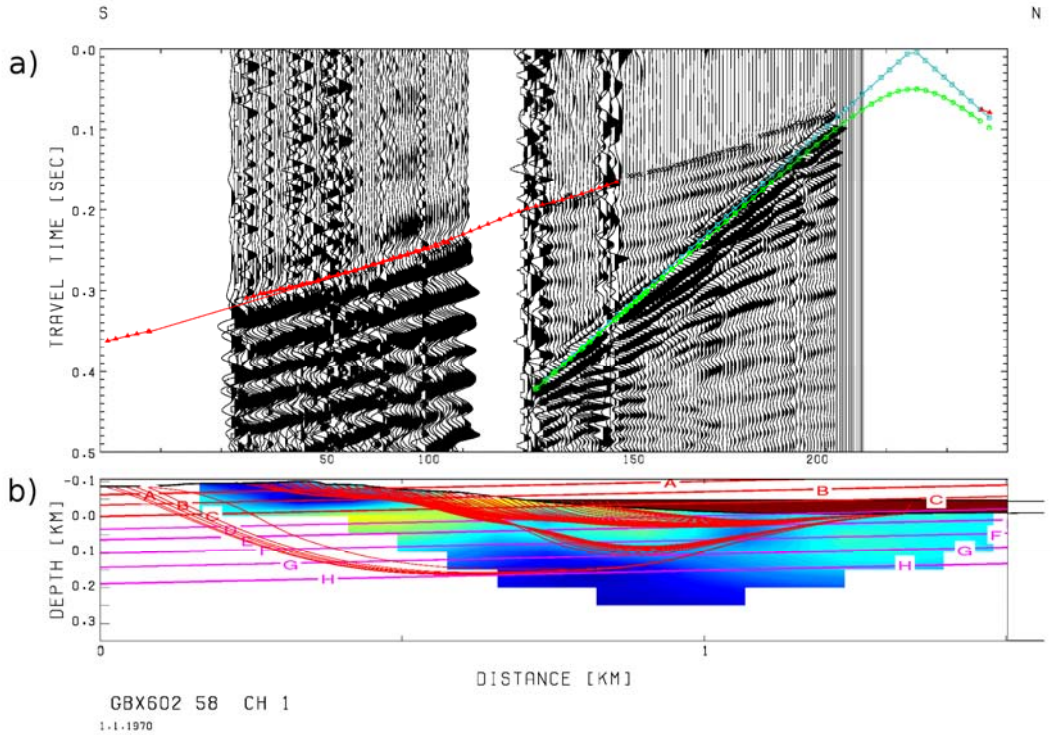

Figure 58 a) Travel times plotted on top of seismic shot gather. b) Ray paths for airgun shot point 58 plotted on top of velocity model. Calculated with *modelfinal04*.

3.4.2 Quantitative correlation to velocity well logs

As part of the SeiFaBa project (Japsen, Andersen, Boldreel, Waagstein, White R.S., Worthington, and The SeiFaBa group 2006) the ~700 m deep Glyvursnes-1 well was drilled. Full-waveform sonic logs in the Glyvursnes-1 boreholes were acquired (Waagstein and Andersen 2003) and VSP experiments were carried out (Shaw 2006).

The logs used for the present analysis are the GEUS processed full waveform velocity logs and the bulk density logs re-calibrated to measurements on core samples (*GL1-FWS_GEUS.LAS* and *gl1-dens.txt*, Waagstein , unpublished data).

3.4.2.1 The VSP and velocity logs

Interval velocities were derived from VSP data by picking of travel times. Ideally the picks should be on the very first onset but it can be difficult to identify the low amplitude. The first zero crossing can not be used due to that the earth filtering effect on the signal introduces too much noise.

Pickings have to be on a well defined feature of the waveform, early on the waveform but late enough so that the waveform has gained some energy. Picking the first maximum gradient of the waveform complies with these demands. The maximum gradient of the recorded signal is equal to the first zero crossing of the second derivative of the signal. Before taking the second derivative the signal is low-pass filtered at 200 Hz (Figure 59 and Figure 60).

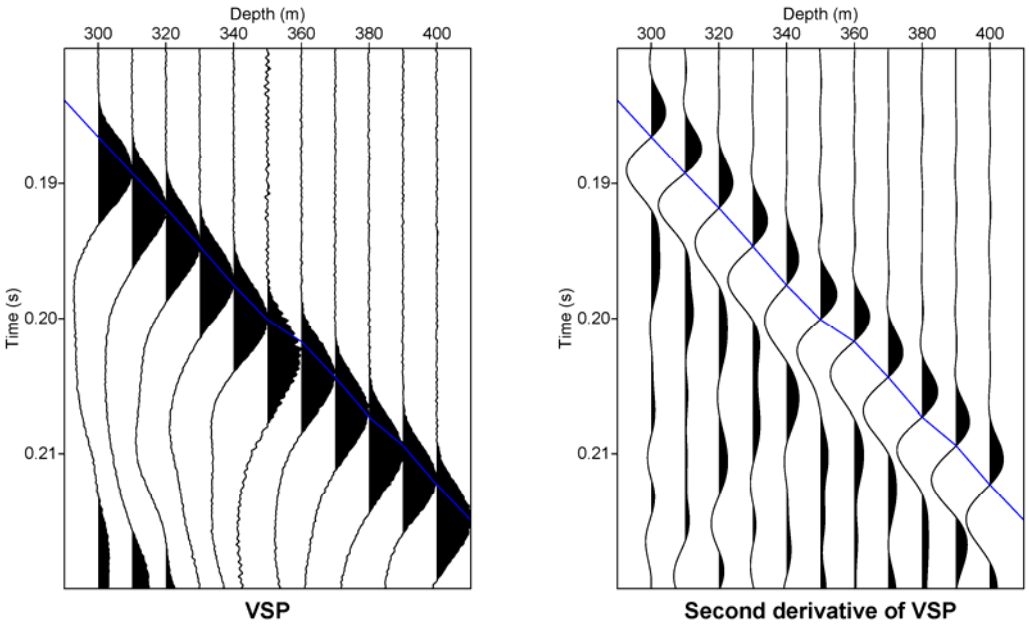

Figure 59 An example of the difference between the raw VSP signal and the second derivative of the filtered VSP signal. Blue line shows the pickings of first zero crossing of the second derivative.

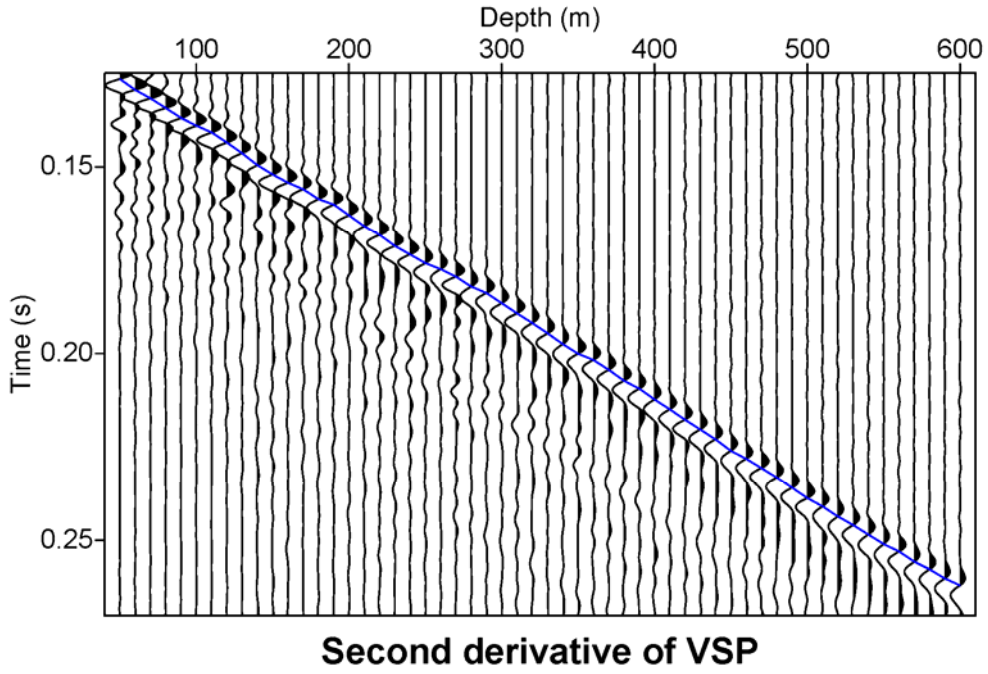

Figure 60 Travel time picks of the full zero offset VSP.

A comparison between the VSP picked travel times and the travel times calculated from the velocity log shows that although there are similarities between the two, the travel times for the velocity log are slightly lower (Figure 61). The difference of ~2.8% is in agreement with Shaw (2006).

I suggest that the difference in travel times is attributed to the very different scales of velocity logs and of VSP signals. The frequency of the signal used for logging was at

23 KHz (Waagstein and Andersen 2003, p. 29) while the signal used for the VSP had a centre frequency of ~33 Hz (Shaw 2006 p. 89)]. In other words, the logged data compares to looking at the world in scales of centimetres whilst the VSP compares to seeing the world in scales of decametres.

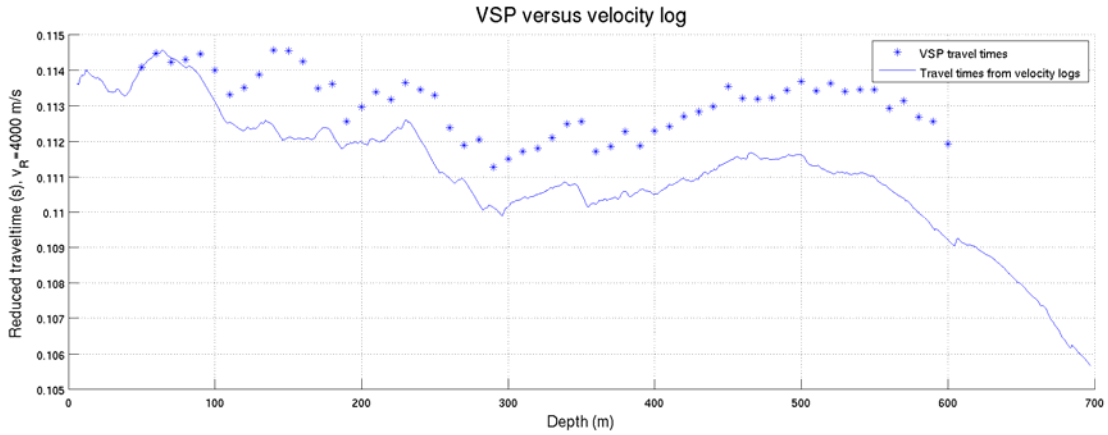

Figure 61. Asterix's show picked travel times on VSP and curve shows the cumulated interval time from velocity log. Plotted with reduced times t_R=t-depth/v_R, v_R=4000 m/s.

Backus (1962) has described the case of a horizontally finely layered medium, where each layer is isotropic or transversely isotropic. When averaged over some height, smaller than the wavelength of a vertical travelling wave, the layered medium can be approximated by a homogeneous transversely isotropic medium where the velocities are algebraic combinations of the velocities and densities of the original medium and the density is the average density for the medium.

So by performing Backus averaging on the velocity logs it is possible to rescale the log values to scales of the VSP seismic signal.

Different intervals for the averaging were tested and the RMS relative to the picked VSP travel times was calculated. The comparison shows that Backus averaging over ~25 m intervals gives the best consistency between logged data and VSP data. This can be interpreted as that the seismic signal used for the VSP in some aspects sees the world in scales of 25 m.

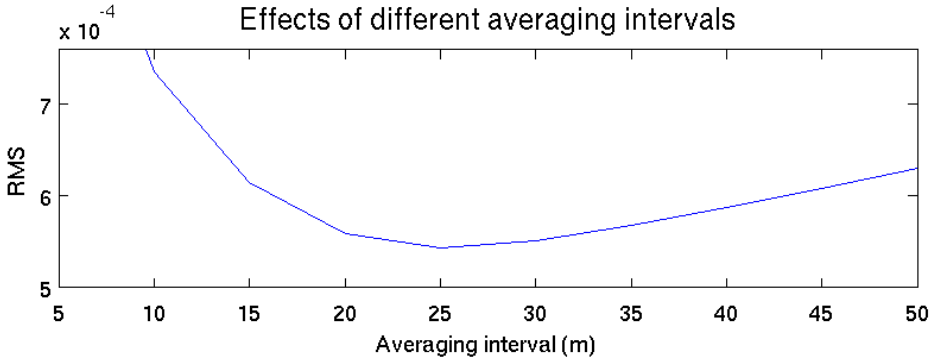

Figure 62. RMS between travel times for VSP and cumulated interval times from velocity log Backus averaged at different intervals.

After applying the 25 m interval Backus averaging, the travel times from the velocity log and from the VSP do correspond very well (Figure 63), and there is still very god

consistency between details of the two. There is however a section in the 100-200 m depth interval where the travel times deviate significantly and consistently.

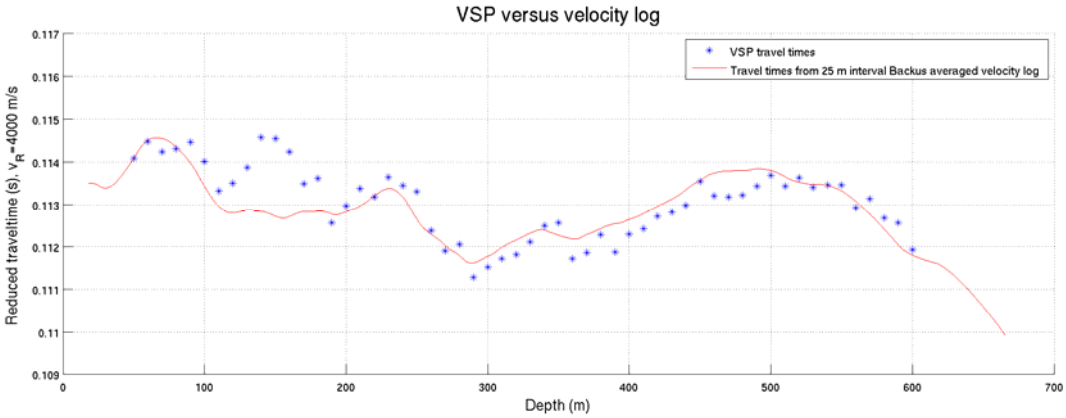

Figure 63. Asterix's show picked travel times on VSP and red curve shows the cumulated interval time after Backus averaging over 25 m intervals. Plotted with reduced times t_R=t-depth/v_R, v_R=4000 m/s.

This can be a matter of the horizontal extent covered by the signal. The full sonic log is affected by properties only in the vicinity of the well location (scales of decimeters) whilst the VSP signal is affected by properties at much larger distance (scales of decameters).

So the difference in the 100-200 m section can be resulting from that the properties in the vicinity of the well are not representative for the larger area around the well. On the other hand we can also say, due to the consistency between VSP and velocity log, that the properties in the vicinity of the well are representative for a larger area around the well at Glyvursnes for most of the depth range.

The VSP travel times can be converted to interval velocities for each 10 m. However the interval velocities are very sensitive to the errors of the picked travel times. A comparison between logged velocities and interval velocities from VSP (Figure 64) show that the VSP velocities have unrealistic high/low values and have a deviation that to a large degree is attributed to uncertainties.

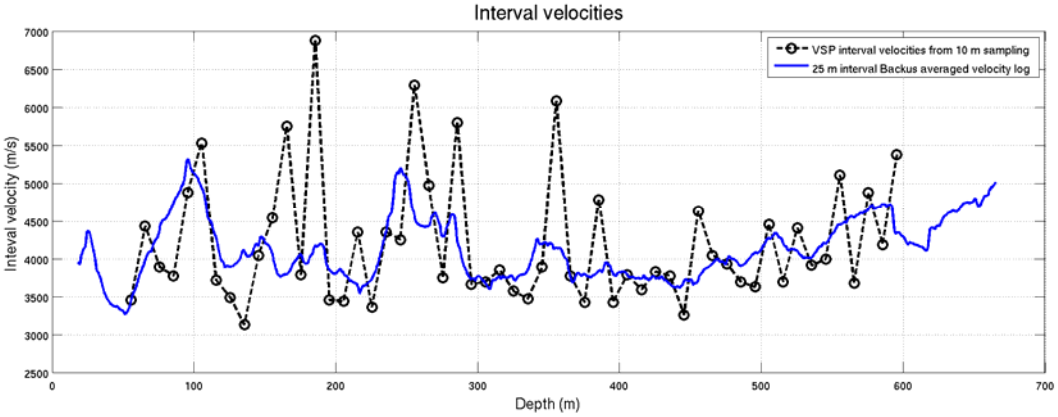

Figure 64 Interval velocities from VSP and from logs.

By calculating interval velocities for 30 m intervals the error level has less significance and a comparison towards the logged velocities shows a good consistency (Figure 65).

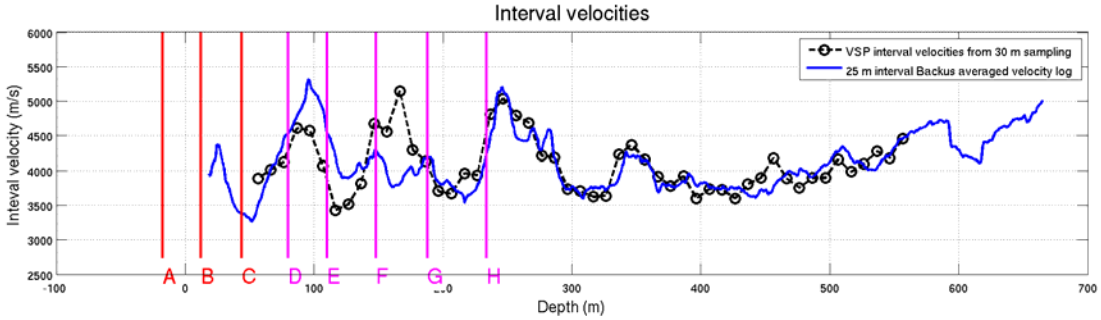

Figure 65 Interval velocities from VSP and from logs. Markers from correlation to geology from above are annotated. Depths are relative to KB.

3.4.2.2 Comparing the modelled profile to VSP and velocity log

The quantitative comparison between modelled velocities and velocities from VSP and logs is obtained by extracting velocities from the model along a cut corresponding to the vertical position of the Glyvurnes-1 well (Figure 66).

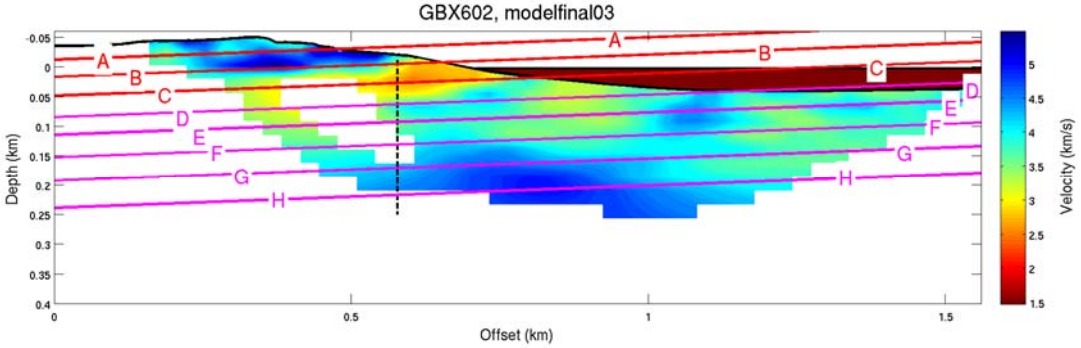

Figure 66 Velocities for comparison to VSP and velocity logs are extracted along the vertical position of the Glyvursnes-1 well (dashed line).

The comparison shows that the details of the 25 m averaged log are not contained in the modelled velocities (Figure 67) although the general trend can be seen. Down to a depth of 0.1 km the modelled velocities are significantly lower (~1 km/s lower for *Modelfinal03*) than the log velocities. In the 0.1-0.18 km interval the velocities are of the same magnitude as the logged velocities. And below they are higher.

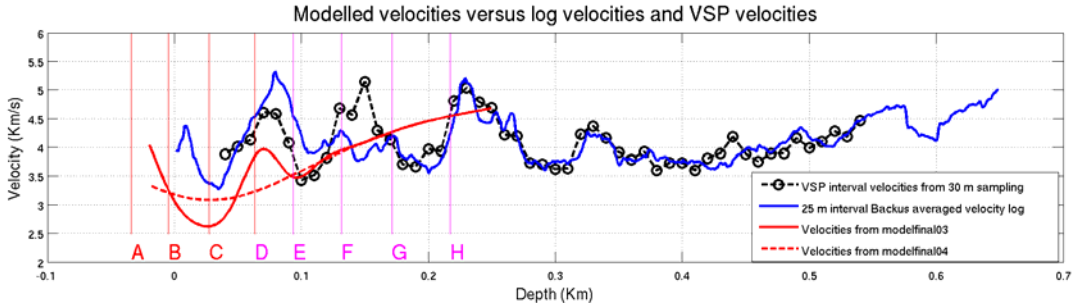

Figure 67 Vertical velocity profile at the location of the Glyvursnes-1 well. Depths are relative to MSL.

However, deeper part of the model at the location of the Glyvursnes-1 well suffers from low ray-density (see ray density distribution Figure 28). Therefore the velocities

were extracted along a second cut and then projected onto the location of the Glyvursnes-1 well using the dip established above from the work of Passey (2005). The location of the second cut was defined primarily on basis of the ray-density distribution (Figure 28) but the details of the modelled profile were also considered (Figure 68).

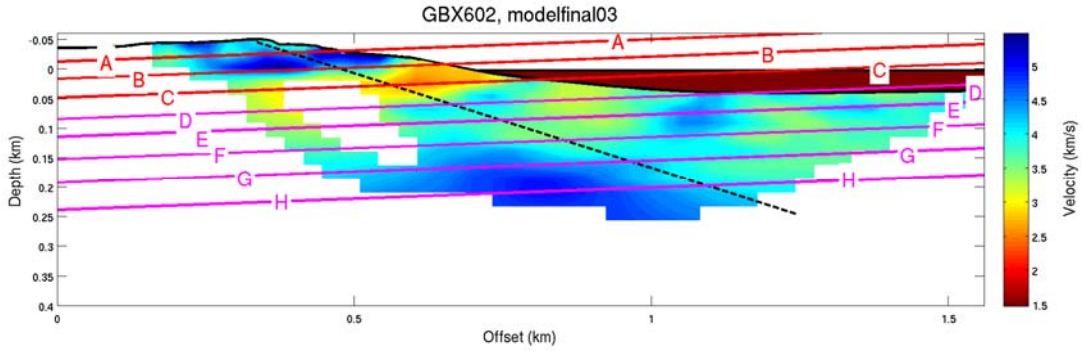

Figure 68 Location of the second cut used for extracting velocities (Black stipulated line).

The magnitude of the velocity difference between velocity log and modelled velocities extracted along the second cut is on about the same scale as for the modelled velocities extracted along the first cut. However, the velocities extracted along the second cut resembles the logged velocities better

The velocities extracted from the coarse model (*modelfinal04*, Figure 30) along the second cut produces velocities that are closer to the logged velocities and have a slightly better localisation of the high/low velocity zones.

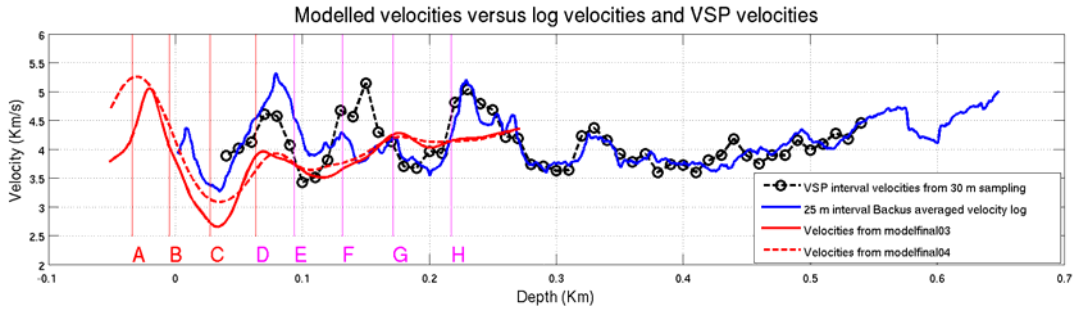

Figure 69 Vertical velocity profile along the second cut projected back onto the location of the Glyvursnes-1 well. Depths are relative to MSL.

A comparison of the vertical and horizontal P-wave velocities at 25 m Backus averaging shows that throughout the total depth, the horizontal P-wave velocity is higher. While in some sections there is little difference there is in other sections a large difference, e.g. in the 0.32-0.35 km depth interval there is a ~0.5 km/s difference (Figure 70).

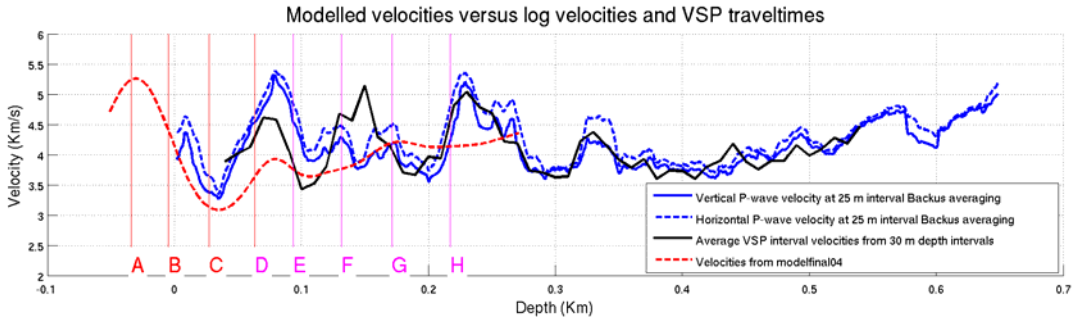

Figure 70 Comparing horizontal and vertical P-wave velocities

A comparison between the VSP velocities and the modelled velocities is equivalent to the comparison between the horizontal and vertical P-wave velocities since the VSP velocities are derived from vertically propagating waves and the modelled velocity are from more horizontally propagating waves. However, the opposite relation turns out to be the case. Comparing the VSP velocities with the modelled velocities shows that the vertical P-wave has higher velocity than the horizontal P-wave (Figure 71).

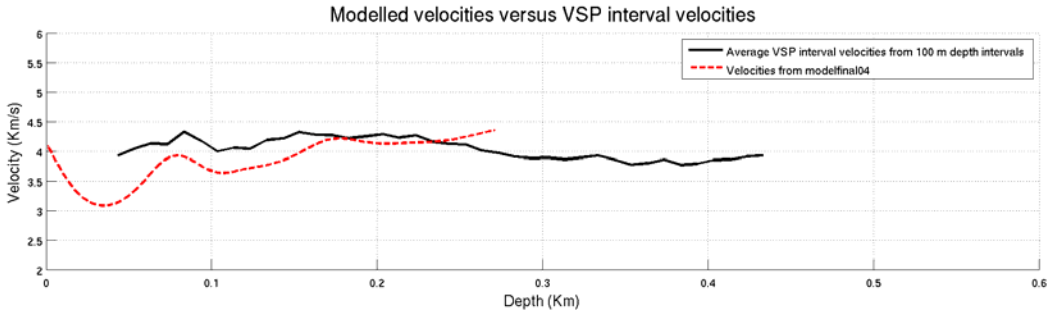

Figure 71 100 m interval average of VSP velocities in order to show same scale of details as the modelled velocities.

Finally, velocities were extracted from the error tests where the streamer was shifted 20 m to the north (Figure 72).

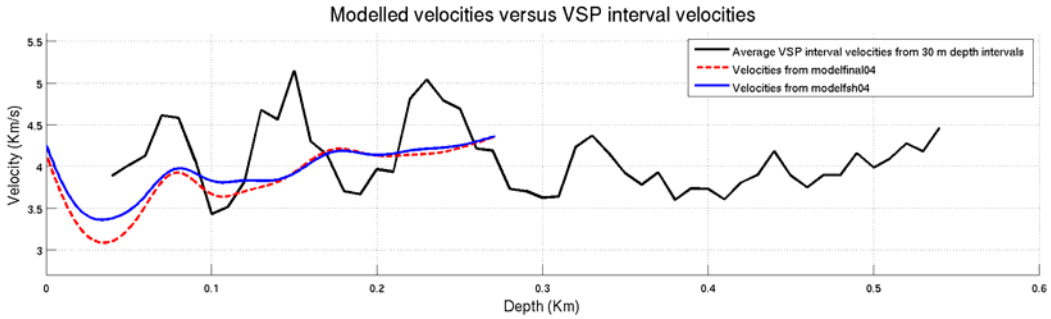

Figure 72 Velocities extracted along the second cut on *Modelfsh04* (Figure 46) and from *Modelfinal04.*

4 Interpretation/Discussion

The profile to model turned out to represent a difficult case to model due to the effects of multiple velocity inversion (high-velocity layer followed by a low-velocity layer) In fact the modelling shows that the uppermost sections of the profile consist of shifts from layers with high velocities to low velocities two or three times (depending on whether VSP interval velocities are consider or log velocities are considered). The uppermost velocity inversion is only detected, by the refraction modelling, as it

crosses the seabed within the profile location and the two next are only identified confidently from the VSP interval velocities and velocity logs (e.g. Figure 70).

The velocity inversions have a deteriorating effect on the ray-coverage as they limit the ray coverage in the deeper parts of the model (e.g. Figure 22, Figure 55 and Figure 56). Further, the high velocity-contrasts of the model results in an uneven ray density distribution with some preferred ray paths. As a consequence, other areas of the model will not have very good constraints on the velocities.

For the inversion a starting model that produces travel times sufficiently close to the picked travel times is needed. The solution is dependent on the starting model, in particular in the case of complex velocity distributions. In the present case no a priori information's were used in generating the starting model.

Judged on the combined convergence of travel times and on the modelling of the uppermost low-velocity zone, the best modelled result was obtained in two steps. First a high VRP (smooth velocity residual, see chapter 3.2) was chosen to get a starting model that produced travel times close to picked travel times. This can be considered to be the actual starting model providing travel times very close to picked travel times. Then the inversion was repeated while minimizing the smoothing effects by setting VRP and OFMP very low.

Continued modelling with the basis in this model did not produce improved models neither when regarding expected behaviour nor when regarding modelled travel times. It turned out that the approach of gradually decreasing the VRP as described by Ditmar *et al.* (1999) did not lead to satisfactory solutions. It is believed that in the present case with the complex velocity distribution, the definition of the *regularization condition* (10 times more restrictive on horizontal changes than on vertical changes) is not beneficial for arriving at solutions by gradual steps. The *regularization condition,* restricting horizontal alteration relative to vertical ones, actually prohibits the developing of the horizontal velocity distribution at continued iterations.

General for the quality of tomography, the angular coverage is an important parameter. That implies equally and densely spaced receiver and shot points. This is often compromised in field experiments. In the present case, the transition from onshore acquisition to offshore acquisition imposes a ~100 m section in the middle of the profile with no receiver or shot point coverage. Also in this area the issue of projecting navigation onto the 2D profile poses the largest effects (Figure 9). The interpretation of the uppermost low-velocity layer should consider that the layer crosses the surface just in the section with missing receiver and shot positions.

Tomographic inversion based on ray theory should consider the effects of the high frequency limit compared to the wavelength of the seismic signal in relation to the structures in the model. As such I have previously advocated for that if the seismic signal is low-pass filtered so all gathers have equal energy in first breaks then an inversion that satisfies all travel times will be a valid solution with scales of resolution compared to the wavelength of the low-pass filtered data (Petersen 2009).

When performing tomographic inversions based on surface seismic data it should also be considered that the needed travel times are only produced in the case of positive vertical velocity gradients. Generally speaking the inversion demands a positive vertical velocity gradient.

The positive vertical velocity gradient is a general property of the subsurface, both small scale and large scale, in areas with sedimentary rocks and complies well with the demands of algorithm of a positive vertical velocity gradient. However, in areas with igneous rocks, as in the current project, this is not at all always the case and the solution should be considered regarding this. It is expected that the demand of a positive vertical velocity gradient will be reflected in the modelled profile.

In the current project there are indications that this effect may have an affect. Down to ~100 m depth the modelled velocities are lower than log velocities while at 100-200 m depth the modelled velocities are of same magnitude as the log velocities (e.g. Figure 69). This can be attributed to that in the upper part of the model the demand of a positive vertical velocity gradient results in the velocities being too low while in the depth interval 100-200 m, representing the general turning point of the ray paths, the velocities are more consistent with the log velocities.

This biasing of the shallow velocities due to the imposed vertical velocity gradient is considered to have a much more serious affect on the modelled result than the mere effect of the high frequency limit modelled by ray theory.

It is clear that, for arriving at a better solution, a better starting model is needed. This could be obtained from the log information and the general dip of layers in the area. The current project is nevertheless a tomographic inversion only based on surface seismic data. Well logs and geological mapping in the area is used as control of the modelled result.

However, if the drawbacks of the method are properly considered, which in the current project means the unequally ray distribution and the imposing of a positive vertical velocity gradient, there are geophysical properties that can be derived directly from the velocity model and that are verified by log and VSP velocities.

Velocities extracted along a cut in the velocity model, which is placed so that it coincides with areas in the model with high ray density, show good conformity with the velocity log (e.g. Figure 69).

Estimation for the general dip in the area can be derived from the uppermos t section in the model (the part of the model covered by marker A to C).

Although the velocity model below marker C does not resemble flow structure and the general dip in the area, the modelled velocity is representative for the velocities of the log and VSP. In areas with high ray coverage velocity information can be related to individual basalt flows (Figure 55, Figure 56, Figure 57 and Figure 58).

The high-velocity zone and the low-velocity zone (marked 1 and 2 in Figure 73) are to some extent interpreted to be related to high-velocity and low-velocity layers crossing the seabed while the vertical extend is considered to be artefacts.

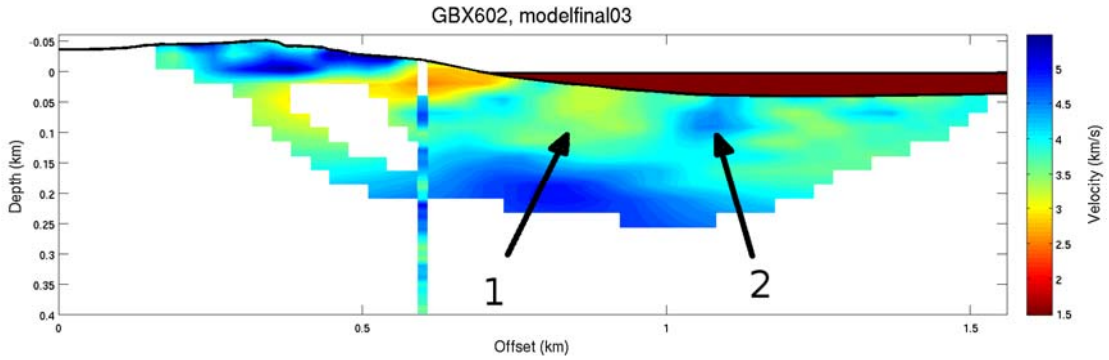

Figure 73 Marking a low-velocity zone (1) and a high-velocity zone (2). The VSP 30 m averaged interval velocity is annotated on top at the location of the Glyvursnes-1 well.

Comparison of the velocity logs and VSP data establishes that Backus averaging of the velocity logs to 25 m interval produces the best conformity between velocity logs and VSP data (Figure 63) when considering total travel times. This result explains the difference in travel times between the cumulated velocity log and travel times from VSP reported by Shaw (2006). It is considered an interesting side benefit of the work. Backus (1962) says that the averaged seismic response is valid for wavelengths much longer than the average interval. A 33 Hz signal (the centre frequency of the VSP signal) has a wavelength of 100-180 m for velocities in the interval 3000-6000 m/s. In the present case the wavelength is thus 5-7 times longer than the averaging interval.

With the basis in a 25 m averaging interval the horizontal P-wave velocity can be calculated from Backus averaging (Figure 70). Over most of the depth range the horizontal P-wave is of approximately same value, but higher, than the vertical P-wave velocity. In a few places, marked F, G, at ~250 m and at 330 m depth, it is significantly higher.

The velocities from VSP data and the velocities from tomographic inversion offer the opportunity to compare the propagation of vertically travelling waves (VSP) to the propagation of almost horizontally travelling waves (surface seismic data). A comparison to VSP interval velocities, derived from 100 m depth intervals, in order to have same scale of details as the modelled velocities, shows that down to 170 m depth, the vertically travelling waves have higher velocity than the horizontally travelling waves (Figure 71). This is opposite to the result from the Backus averaging to 25 m intervals. In the 170-230 m depth interval the velocities are of same magnitude.

Before more weight can be put on this result further verification is necessary. Firstly it would be to confirm the travel times of the model with full waveform modelling and secondly to test other obvious models (derived from logs).

Although this results needs further verification it shall be mentioned that it is in line with Kiørboe and Petersen (1995) reporting a 10% lower horizontal P-wave velocity in the uppermost 800 m in connection with the Lopra well. They suggest that the lower horizontal velocity could be connected to fractures around basalt columns and possibly in combination with nearly vertical master joints.

5 Conclusions

As shown above, the modelling succeeds in producing a velocity profile down to ~200 m depths at the centre of the profile.

In areas of the profile, where the layers are crossing the surface with a sufficient slope, high-velocity and low-velocity zones are uniquely determined whilst below that the velocities are determined to the general magnitude but the exact locations of high- and low-velocity zones can not considered being uniquely determined.

The velocities in the upper part of the model could be too low as a result of the modelling method or of the uncertainties involved in the data. Further verification is needed in the form of travel times modelled by full waveform modelling and by travel times by alternative models.

Different inversion parameters lead to different solutions. Although there are great similarities, the location of high and low velocity zones may vary. Imposing errors on the input data, when performing error estimates, did in no case lead to a different solution, when the inversion was performed with same parameters. That means, although velocity magnitudes did vary a little, the location of high/low velocity zone was consistent for all results. This shows that the solutions are stable relative to uncertainties relating to data.

This project demonstrates that the presented method is useful for deriving velocities in the uppermost sections of basalt covered areas. The parameters used for this particular modelling, i.e. gridding, VRP and OFMP, can be used as guidance for other profiles in the area. The limitation of ray tracing based inversion is in this particular case mainly the imposing of a positive vertical velocity gradient.

It must nevertheless be stated that we fail to model the continued velocity distribution of basalt flows in a convincing manner. The modeled velocity distribution shows signs of being affected by the ray tracing putting more weight on certain areas due to unequal ray density distribution.

6 Future plans

As a first step, before the results are ready for further publishing, it most be verified that the relative low velocities in the upper part of the model are not just an artefact. The verification will be two fold. Firstly by travel times from full waveform modelling and secondly by travel times from alternative models based on the velocity log and general dip in the area.

If travel times from full waveform modelling are consistent with seismic data and if alternative solutions do not produce better results, then there is better basis for considering the relatively low velocities in the upper part of the model to be a real property of the area and not an artificial effect. This work will be undertaken right away.

With the basis in the modelled velocities the combined profile will be processed to stack. The processing will aim towards enhancing the shallow sections. To obtain this

prestack migration and prestack redatuming of data will be the central issues of the processing. This work will be undertaken as soon as possible.

The current project leads to the suggestion of some projects to continue the work:

Project 1:
The use of refraction seismic tomography to identify the location of the low-velocity layer related to Argir Beds directly from seismic data. The current project demonstrates that this is possible in areas where the low-velocity zone crosses the seabed with a sufficient slope.

From the GlyvVest 2007 survey there exist profiles passing close by Glyvursnes in Nólasoyarfjorð and on the other side of Streymoy passing by Kirkjubø. These profiles intersect south of Streymoy (Figure 74).

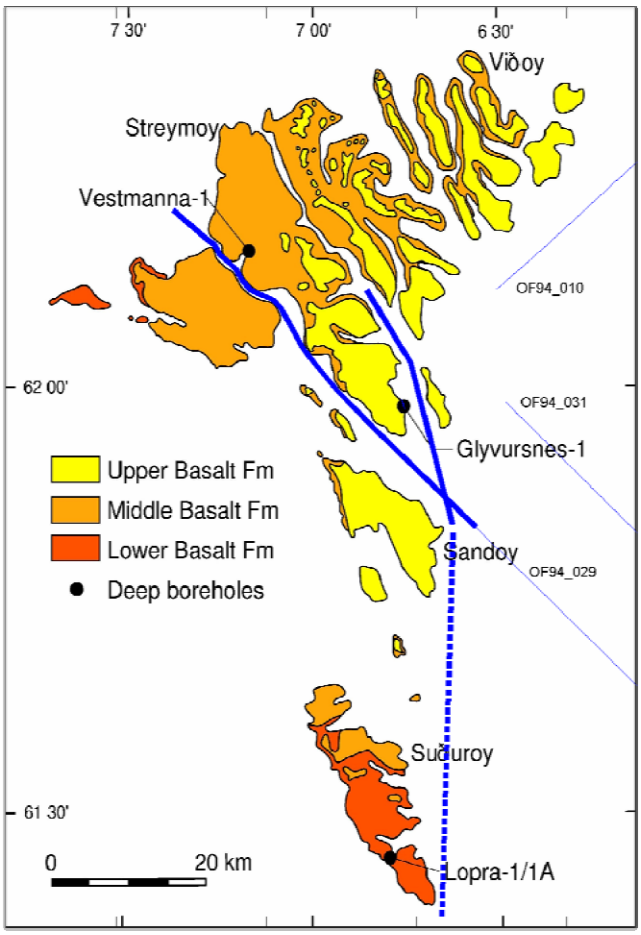

Figure 74 From the GlyvVest 2007 proposal outlining the suggested profiles. These were all acquired successfully. An extra profile connecting to the OF94_010 was also acquired.

The general strike and dip of flows in the area from surface mapping (e.g. Passey 2005) can be extrapolated on to the profiles to get an estimated location of Argir Beds. The exact location of the crossing with seabed can then be determined by refractions seismic tomography.

The aim will be two fold: firstly providing a geological marker for the seismic profiles and secondly closer studying of the seismic response of Argir Beds.

The GlyvVest profiles connect to several profiles from the OF94 survey. The geological identification of reflections on the GlyvVest profiles does thus provide the opportunity to extrapolate geological information from the Glyvursnes well onto the profiles from the OF94 survey and thereby linking known onshore geology to imaged offshore geology.

The GlyvVest data are acquired by NVD (Náttúruvísindadeildin, Fróðskaparsetur Føroya) and is the basis for the ongoing work by Hilmar Simonsen and Khanh Duc Nguyen at NVD. The suggested project would be a supplement to the work by Hilmar and Khanh.

Project 2:
Anisotropy study on the basis of three airgun-geophone profiles from the SeiFaBa 2003 survey (GA, GB and GC, see Andersen, Worthington, Mohammed, White, Shaw, and Petersen 2004). The profiles are oriented in a range of 90 degrees centred at the Glyvursnes-1 well. Only the shot profiles inline with the geophone layouts are considered (Figure 75). The geophone layouts are all 400 m long with 5 m stations interval and every fourth being a 3C geophone. The interval of the shooting profiles ranges from 2-4 km and the total offsets ranges from 3-5 km. Also all shots where recorded on a 3C downhole geophone at 400 m depth in the Glyvursnes-1 well.

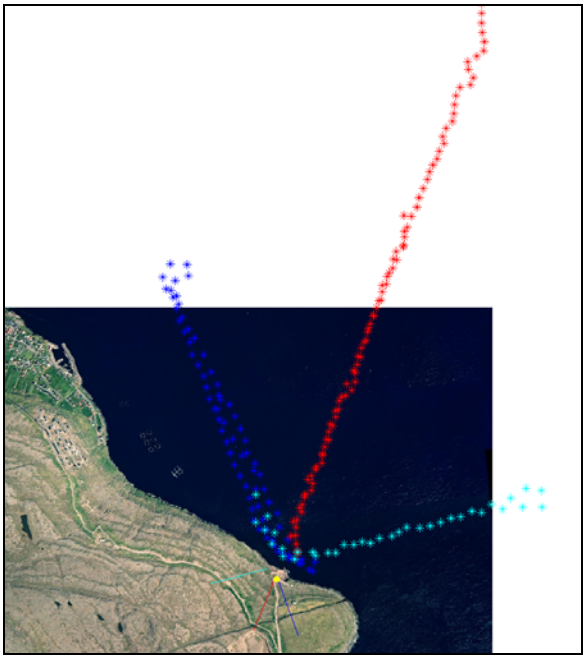

Figure 75 Solid lines: Geophone layout for GAX, GBX and GCX (red, blue and magenta). Points mark shot positions for profiles inline with geophone layout (Respectively same colours). Yellow dot marks location of Glyvursnes-1 well.

The data only involve one-way shooting which is known for being a critical factor in refraction tomography. A further diminishing factor is that the data do generally not contain near offsets. However, a comparison to the current modelled profile, which is also recorded on the GB geophone layout, would function as a verification of the method.

The inversion will be performed with the use of Warrpi as demonstrated in this project. Warrpi also facilitates the inversion of downhole data, either as separated models or included in the surface seismic data.

This project will enable the studying of anisotropy both from horizontally layers and from vertical fractures (VTI and HTI anisotropy parameters).

7 Acknowledgements

First of all I want to thank all the driving forces behind the SeiFaBa project, in particular Morten S. Andersen for the surface seismic acquisition, which resulted in the data for this project. The data also have the potential for many future studies. I also want to thank Michael Worthington for being help full with the VSP data.

Thanks to:

- Robert J. Brown for discussions on wave propagation and on convention of recordings.
- Turid Madsen and Romica Øster at Jarðfeingi for assisting me in the re-measuring of positions at Glyvursnes and to Anne Marie Nordby at Landsverk.
- Per Trinhammer at Aarhus Universitet for helping me with questions on the navigation logs.
- Thomas Varming and Heri Ziska for discussions and proofreading.
- Jannis Makris at Geopro for helping with questions on Warrpi and on refraction tomography.

Reference List

1. Andersen, M. S., Worthington, M., Mohammed, N. G., White, R. S., Shaw, F., and Petersen, U. K. Seismic Experiments at Glyvursnes, Juni -December 2003, Aquisition report. 37. 2004. Geological Survey of Denmark and Greenland. Ref Type: Report

2. BACKUS, G. E. 1962. Long-Wave Elastic Anisotropy Produced by Horizontal Layering. *Journal of Geophysical Research* **67**(11), 4427-&.

3. Brook, R. A., Landrum, R. A., and Sallas, J. J. Report to the SEG Technical Standards Committee regarding proposed polarity convention for vibratory source/recording systems. 1993. Tulsa. Society of Exploration Geophysicists. Ref Type: Report

4. Cerveny V. and Psencik I. SEIS83 - Numerical modeling of seismic wave fields in 2-D laterally varying layered structures by the ray method. E.R.Engdahl. Documentation of Earthquake Algorithms Report SE-35, 36-40. 1984. Boulder.

Documentation of Earthquake Algorithms.
Ref Type: Report

5. CERVENY, V., SOARES, J. E. P. 1992. Fresnel Volume Ray Tracing. *Geophysics* **57**(7), 902-915.

6. DITMAR, P., PENOPP, J., KASIG, R., MAKRIS, J. 1999. Interpretation of shallow refraction seismic data by reflection/refraction tomography. *Geophysical Prospecting* **47**(6), 871-901.

7. GALLAGHER, J. W., DROMGOOLE, P. W. 2008. Seeing below the basalt - offshore Faroes. *Geophysical Prospecting* **56**(1), 33-45.

8. Japsen, P., Andersen, M. S., Boldreel, L. O., Waagstein, R., White R.S., Worthington, M., and The SeiFaBa group. Seismic and petrophysical properties of Faroes basalts (the SeiFaBa project Final Report). 29. 2006. Geological Survey of Denmark and Greenland.
Ref Type: Report

9. KIØRBOE, L., PETERSEN, S. A. 1995. Seismic investigation of the Faeroe basalts and their substratum., 111-122.

10. Passey, S. R. Geology of Glyvursnes, Streymoy, Faroe Islands. A contribution to the SeiFaBa project. Funded by the Sindri Group. 20-6-2005.
Ref Type: Report

11. Petersen, U. K. Reflection seismic data used for refraction analysis giving information of the small-scale velocity distribution of near-surface basalt flows. 2009.
Ref Type: Report

12. PETERSEN, U. K., ANDERSEN, M. S., WHITE, R. S. 2006. Seismic imaging of basalts at Glyvursnes, Faroe-Islands – Hunting for future exploration methods in basalt covered areas. *First Break* **24**(March 2006).

13. PHILLIPS, W. S., FEHLER, M. C. 1991. Traveltime Tomography - A Comparison of Popular Methods. *Geophysics* **56**(10), 1639-1649.

14. SHAW, F. 2006. Seismic properties of Faroe Island basalts. *DPhil*.

15. THIGPEN, B. B., DALBY, A. E., LANDRUM, R. 1975. Special Report of Subcommittee on Polarity Standards. *Geophysics* **40**(4), 694-699.

16. VASCO, D. W., PETERSON, J. E., MAJER, E. L. 1995. Beyond Ray Tomography - Wavepaths and Fresnel Volumes. *Geophysics* **60**(6), 1790-1804.

17. Waagstein, R. and Andersen, C. Well completion report: Glyvursnes-1 and Vestmanna-1, Faroe Islands. 99. 2003. Copenhagen, Geological survey of Denmark and Greenland.
Ref Type: Report

18. WHITE, R. S., SMALLWOOD, J. R., FLIEDNER, M. M., BOSLAUGH, B., MARESH, J., FRUEHN, J. 2003. Imaging and regional distribution of basalt flows in the Faeroe-Shetland Basin. *Geophysical Prospecting* **51**(3), 215-231.

19. WILLIAMSON, P. R. 1991. A Guide to the Limits of Resolution Imposed by Scattering in Ray Tomography. *Geophysics* **56**(2), 202-207.

20. WILLIAMSON, P. R., WORTHINGTON, M. H. 1993. Resolution Limits in Ray Tomography Due to Wave Behavior - Numerical Experiments. *Geophysics* **58**(5), 727-735.

21. ZIOLKOWSKI, A., HANSSEN, P., GATLIFF, R., JAKUBOWICZ, H., DOBSON, A., HAMPSON, G., LI, X. Y., LIU, E. R. 2003. Use of low frequencies for sub-basalt imaging. *Geophysical Prospecting* **51**(3), 169-182.